A PASSIVE WIRELESS TEMPERATURE SENSOR FOR HARSH ENVIRONMENT APPLICATIONS

by

YA WANG

A thesis submitted in partial fulfillment of the requirements for the degree of

MASTER OF SCIENCE
in
MECHANICAL ENGINEERING

UNIVERSITY OF PUERTO RICO
MAYAGÜEZ CAMPUS
2007

Approved by:

_____	_____
Frederick Just-Agosto, PhD Member, Graduate Committee	Date
_____	_____
Manuel Toledo-Quiñones, PhD Member, Graduate Committee	Date
_____	_____
Yi Jia, PhD President, Graduate Committee	Date
_____	_____
Noel Artiles-Leon, PhD Representative of Graduate Studies	Date
_____	_____
Paul Sundaram, PhD Chairperson of the Department	Date

ABSTRACT

High temperature sensors suitable for operating in harsh environments are needed in order to prevent disasters caused by structure or system functional failures due to elevated temperatures, for example, temperature monitoring of heat resistant tiles of the space shuttle and temperature monitoring of rotating bearings in the aircraft engine. Most existing temperature sensors do not satisfy the needs because these sensors require either physical contact or a battery power supply for signal communication, and furthermore, neither of which can withstand high temperatures nor rotating applications.

A novel passive wireless temperature sensor, being able to operate in harsh environments, has been developed in this research project for high temperature rotating component applications. A completely passive *LC* resonant telemetry scheme, which relies on a frequency shift output, has been integrated with the sensor, thereby eliminating the needs for contacts, active elements, or power supplies within the sensor. Consisting of an inductor and a temperature-dependent capacitor, this high temperature sensor forms a *LC* circuit, whose resonant frequency changes when the capacitance of the sensor changes in response to temperature.

Following a review of the state-of-the-art high temperature dielectric ceramics and substrates, schematic design of the capacitor was presented based on temperature sensitive ferroelectric dielectrics. These dielectrics were found to exhibit linear changes in electrical properties when exposed to temperature varying environments. Based on capacitance and inductance modeling and simulation, sensor design and modeling was conducted subsequently in order to limit the resonant frequency to the appropriate scope.

Moreover, sensor performance was analyzed to optimize the sensor configuration, maximize sensing distance, *Q* factor and sensitivity. The sensor prototype was then successfully fabricated to prove the concept of a temperature sensing device using passive wireless communication. The Low Temperature Co-fire Ceramic (*LTCC*) technology based on DuPont Green Tape ™ was proposed for sensor packaging. Finally, the sensor prototype was calibrated up to 235ºC in a laboratory setup.

RESUMEN

Los sensores de alta temperatura adecuados para operar en ambientes desfavorables son necesarios para prevenir desastres causados por fallos de estructura o fallos funcionales del sistema debido a las altas temperaturas, como por ejemplo, para monitorear la temperatura de baldosas resistentes al calor del transbordador espacial y monitorear la temperatura de los cojinetes rotantes en el motor de un avión. La mayoría de los sensores de temperatura existentes no satisfacen estas necesidades porque estos sensores requieren o bien contactos físicos o un suministro de energía por batería para la comunicación por señal, y adicionalmente, ninguno de estos puede soportar altas temperaturas ni aplicaciones rotatorias.

Un nuevo sensor pasivo inalámbrico, capaz de operar en ambientes adversos, fue desarrollado en este proyecto de investigación para aplicaciones a componentes rotantes a altas temperaturas. Un esquema de telemetría resonante *LC* completamente pasiva, el cual se basa en un cambio en la frecuencia de salida, ha sido integrado con los sensores, por consiguiente eliminando la necesidad de que contactos, elementos activos o fuentes de energía contenidos en el sensor. Compuesto de un inductor y un capacitor dependiente de la temperatura, este sensor de alta temperatura forma un circuito *LC*, cuya frecuencia de resonancia cambia cuando la capacitancia del sensor varía en respuesta a la temperatura.

Siguiendo una revisión de la más moderna tecnología en cerámicas dieléctricas de alta temperatura y substratos, un diseño esquemático del capacitor fue presentado basándose en dieléctricos ferroeléctricos sensibles a la temperatura. Se ha encontrado que estos

dieléctricos exhiben cambios lineales en las propiedades eléctricas cuando se exponen a ambientes en los que cambia la temperatura. Basado en el modelado y simulación de inductancia y capacitancia, se condujo un diseño esquemático subsecuentemente con el fin de limitar la frecuencia resonante al campo de acción apropiado.

Más aún, el desempeño del sensor fue analizado para optimizar la configuración del sensor, maximizar la distancia de sensado, el factor Q y la sensibilidad. El prototipo del sensor fue entonces fabricado exitosamente para probar el concepto de un aparato de medición de temperatura usando comunicación inalámbrica pasiva. La Cerámica de Baja Temperatura Co-fire (*LTCC*) basada en la tecnología DuPont Green Tape TM fue propuesta para el empaquetamiento del sensor. Finalmente, el prototipo de sensor fue calibrado hasta 235 °C en un montaje de laboratorio.

ACKNOWLEDGEMENTS

I wish to express my gratitude to my thesis advisor, Professor Yi Jia, for his advice and support throughout this thesis project. I feel grateful for having been offered a chance to study novel sensor development in his research group. I am also grateful for his continuous support and encouragement that helped me overcome the disappointments during my research work.

I would like to thank Dr. Fredrick Just for providing with the laboratory equipment required for the experimental part of my thesis. I would like to express my special thanks to him for his patience in explaining control problems as I worked as a TA in his automatic control class. In addition, I would like to thank Dr. Toledo-Quiñones for his supportive encouragements as a member of my graduate committee.

At last, but the most importantly, I would like to thank my family, for their unconditional support, inspiration and love.

Funding and resources for the development of this research were provided by NSF Grant 0549338 and DE-FG26-07NT43061.

Table of Contents

ABSTRACT ..... **I**

RESUMEN ..... **III**

ACKNOWLEDGEMENTS ..... **V**

LIST OF TABLES ..... **VIII**

LIST OF FIGURES ..... **IX**

INDEX OF SYMBOLS ..... **X**

1 INTRODUCTION ..... **- 1 -**

1.1 BACKGROUND ..... - 1 -
1.2 PROPOSED PASSIVE WIRELESS TEMPERATURE SENSOR ..... - 3 -
1.3 ADVANTAGES OF THE PASSIVE WIRELESS SENSOR ..... - 4 -
1.4 RESEARCH OBJECTIVES ..... - 4 -
1.5 THESIS ORGANIZATION ..... - 5 -

2 LITERATURE REVIEW ..... **- 6 -**

2.1 HIGH TEMPERATURE THERMOCOUPLES ..... - 6 -
2.2 HIGH TEMPERATURE OPTICAL SENSORS ..... - 7 -
2.3 HIGH TEMPERATURE *SAW* SENSORS ..... - 8 -
2.4 *RF* POWERED *LC* SENSORS ..... - 9 -
2.5 CONCLUSIONS ..... - 10 -

3 SENSOR DESIGN AND SIMULATION ..... **- 11 -**

3.1 DESIGN PRINCIPLE ..... - 11 -
3.2 PLANAR CAPACITOR ..... - 12 -
3.3 SPIRAL INDUCTOR ..... - 14 -
3.4 ELECTRICAL MODEL OF RESONANT CIRCUIT ..... - 16 -
3.5 CONCLUSIONS ..... - 21 -

4 HIGH TEMPERATURE SENSITIVE MATERIALS ..... **- 22 -**

4.1 HIGH TEMPERATURE CERAMIC MATERIALS ..... - 22 -
4.1.1 Beryllium Oxide (BeO) ..... *- 23 -*
4.1.2 Aluminum Nitride ..... *- 24 -*
4.1.3 Alumina ..... *- 25 -*
4.1.4 Macor ..... *- 25 -*
4.2 PIEZOELECTRIC MATERIALS ..... - 25 -
4.2.1 Ferroelectricity ..... *- 26 -*
4.2.2 Lead Zirconate Titanate (PZT) ..... *- 28 -*
4.2.3 Lead Lanthanum Zirconate Titanate (PLZT) ..... *- 29 -*
4.2.4 Lead Nb Zirconate Titanate (PNZT) ..... *- 29 -*
4.2.5 Lead Bi Lanthanum ZirconateTtitanate (PLBZT): ..... *- 30 -*
4.3 CONCLUSIONS ..... - 31 -

5 SENSOR PERFORMANCE ANALYSIS ..... - 33 -

5.1 MODELING AND SIMULATION ..... - 33 -
5.2 PERFORMANCE ANALYSIS ..... - 38 -
5.2.1 Resonant Frequency ..... - 38 -
5.2.2 Q-factor ..... - 40 -
5.2.3 Coupling Factor ..... - 42 -
5.3 CONCLUSIONS ..... - 43 -

6 SENSOR FABRICATION ..... - 45 -

6.1 SENSOR PROTOTYPE ..... - 45 -
6.2 SENSOR PACKAGE ..... - 46 -
6.3 CAPACITANCE MEASUREMENT ..... - 47 -
6.3.1 Oscillations of the RLC Circuit ..... - 47 -
6.3.2 Performing the Experiment ..... - 49 -
6.4 SENSOR CALIBRATION ..... - 52 -
6.5 CONCLUSIONS ..... - 54 -

7 CONCLUSIONS AND FUTURE WORK ..... - 55 -

7.1 CONCLUSIONS ..... - 55 -
7.2 FUTURE WORK ..... - 56 -

List of Tables

Tables **Page**

Table 4-1 Mechanical Properties Comparison (25ºC, 1 kHz) .....- 23 -
Table 5-1 System Parameter Values (at 20 ºC).....- 37 -

List of Figures

Figures **Page**

Figure 1.1 Proposed Wireless Temperature Sensing System ..... - 2 -
Figure 1.2 the Proposed Wireless Sensor Scheme ..... - 3 -
Figure 3.1 Schematic Diagram of Temperature Sensor ..... - 11 -
Figure 3.2 Capacitance *vs.* Dielectric Constant ..... - 13 -
Figure 3.3 Schematic View of Spiral Inductor ..... - 14 -
Figure 3.4 Inductance *vs.* Coil Mean Radius ..... - 16 -
Figure 3.5 Inductively Coupled Circuit ..... - 17 -
Figure 3.6 Resonant Frequency *vs*. Dielectric Constant ..... - 20 -
Figure 4.1 Dielectric Constant Variation Comaprison ..... - 24 -
Figure 4.2 Dielectric Constant *vs.* Temperature of *PZT* ..... - 28 -
Figure 4.3 Dielectric Constant *vs.* Temperature of *PLZT* ..... - 29 -
Figure 4.4 Dielectric Constant *vs.* Temperature of *PNZT* ..... - 30 -
Figure 4.5 Dielectric Constant *vs.* Temperature of *PLBZT* ..... - 31 -
Figure 5.1 Inductive Coupled Reader and *LC* Sensor ..... - 33 -
Figure 5.2 Equivalent Circuit Diagram of Wireless Telemetry System ..... - 34 -
Figure 5.3 Magnitude & Phase Angle of Z_S' ..... - 36 -
Figure 5.4 Resonant Frequency of Input Impedance *vs.* Temperature ..... - 38 -
Figure 5.5 *Q*-factor *vs.* Resistance & Inductance ..... - 41 -
Figure 5.6 Coupling Coefficient *vs.* Reader Antenna Radius & Radius Ratio ..... - 43 -
Figure 6.1 Sensor Prototype and Equivalent Circuit ..... - 45 -
Figure 6.2 *LC* Sensor Package (Single Coil) ..... - 46 -
Figure 6.3 Voltage *vs.* Sweep Frequency ..... - 48 -
Figure 6.4 Impedance Variation ..... - 50 -
Figure 6.5 Voltage *vs.* Sweep Frequency ..... - 51 -
Figure 6.6 Capacitance *vs.* Temperature ..... - 52 -
Figure 6.7 Principle of Sensor Calibration Experiment ..... - 53 -
Figure 6.8 Sensor Calibration ..... - 54 -

Index of Symbols

SYSMBOL	NAME	UNIT
A	Sensing area of the sensor	mm^2
a	Coil wire radius	mm
C_R	Capacitance of the reader	F
C_S	Capacitance of the sensor	F
f	Resonant frequency	Hz
I_1	Current on the reader antenna	A
I_2	Current on the sensor	A
k	Coupling Coefficient	/
L_R	Inductance of the reader	H
L_S	Inductance of the sensor	H
M	Mutual inductance	H
n	Turns of the coil	/
R	Coil loop radius	mm
R_R	Self resistance of the reader	Ω
R_S	Self resistance of the sensor	Ω
t	Thickness of the sensing material	mm
T_c	Curie temperature	K
ε_0	Permittivity of free space 8.85×10^{-12}	F/m
μ_0	Magnetic permeability of free space $4\pi \times 10^{-7}$	H/m

1 INTRODUCTION

This chapter starts with the background introduction of this thesis project, followed by the proposed novel passive wireless temperature sensor description for harsh environment applications, and finally an overview and organization of the thesis is presented.

1.1 Background

In order to prevent disasters caused by structure failures in high temperature environments, reliable high temperature sensing devices are needed, for example, for temperature monitoring of heat resistant tiles of the space shuttle, temperature testing of rotating bearings in the aircraft engine, and qualification testing of disc brakes, jet engine dynamics and high-speed shaft rotations [1-4].

However, most existing temperature sensors offering outstanding performance in static and room temperature applications suffer from severe performance degradation and failure above 130 ºC [5]. Many technologies have been proposed in order to improve application in harsh environments, such as Silicon on Insulator (*SOI*) and Silicon Carbon (*SIC*) based device technologies, which appear promising for operations reaching 300 ºC and 600 ºC respectively [6-8]. But all these electronic semiconductor systems require a power supply, which will result in significant power dissipation. This is undesirable for high-temperature applications where a power source is highly limited. Because batteries such as solid state lithium batteries suffer from severe performance degradation at high temperatures, they are limited by electrochemical process constraints [9]. Miniature high-temperature batteries are still under development [10]. Thermoelectric generators have been proposed to convert temperature gradients in a high-temperature environment to a *DC* power [11]. But

this approach can only be applied within a limited temperature range and may require a complex wiring setup to ensure proper temperature gradients. Furthermore, these devices require feed-through wires to reach an external power supply as well as signal communications, which severely limits the system flexibility and performance. In order to remove the need for electronics, power supplies, or physical contacts, the wireless sensor technologies draw many attentions, for example, wireless sensor development for pressure monitoring [12-14].

In this thesis, a novel passive wireless temperature sensor based on planar resonator and thick film technologies was proposed and developed. As illustrated in Figure 1.1, the proposed sensor was designed attachable on rotating component to measure temperature changing. The remote portable reader detected the temperature variation by monitoring the impedance across the terminals of the wide bandwidth reader antenna. And then this temperature information is received through a reader and interpreted by Laptop computer in terms of resonant frequency.

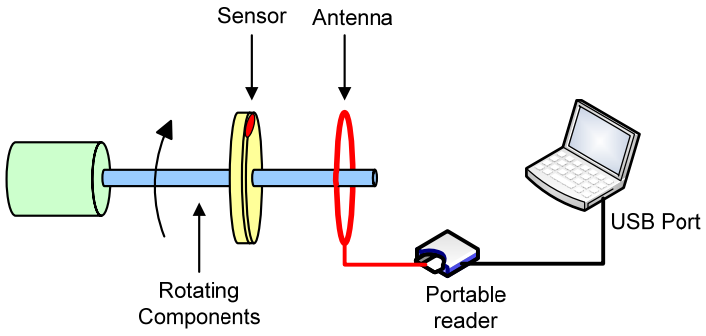

Figure 1.1 Proposed Wireless Temperature Sensing System

1.2 Proposed Passive Wireless Temperature Sensor

This innovative *LC* temperature sensor, together with the remote reader, will accomplish high-temperature monitoring, integrating high temperature ceramic materials instead of traditional off-the-shelf electronic components. The temperature signal is coupled with the resonant frequency acquired by the remote antenna, which carries out the function of remote power supply and wireless communication.

The power delivery and wireless data communication is presented and illustrated in Figure 1.2. The sensor is powered by a remote reader which sends out an oscillating magnetic field across reader antenna and sensor inductor by inductive link. The measured temperature changes induced the variation of sensor capacitance due to the temperature-sensitive dielectric material of the capacitor. The remote reader detected this temperature information by monitoring resonant frequency variation due to impedance changes in response to temperatures.

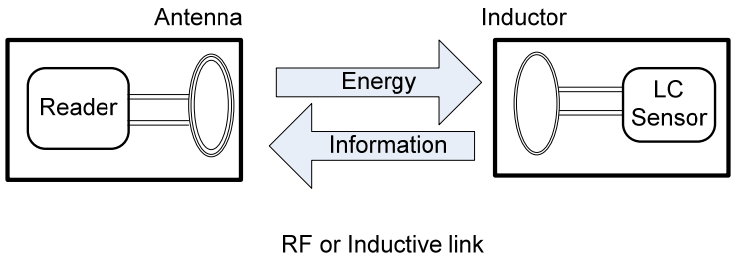

Figure 1.2 the Proposed Wireless Sensor Scheme

1.3 Advantages of the Passive Wireless Sensor

The technology developed in this research project will extend the basic knowledge of passive wireless sensing, high temperature sensitive materials and associated prognostic health monitoring technologies in harsh environment conditions. The resulting sensor will offer many extraordinary features such as compact size, a contact-less power supply, wireless data communication, resistance in high temperature rotating component monitoring and low cost. The advantages of the proposed wireless sensing system can be summarized as follows:

(1) Remove physical contacts and electronics;

(2) Create a capacitive frequency-encoded sensing mechanism based on LC circuit;

(3) Extend the high temperature sensor application of ferroelectric materials;

(4) Integrate a wireless sensor and inductive powering into one multilayer structure;

(5) Come true sensor operation for high temperature rotating component monitoring.

1.4 Research Objectives

The primary objective of this project is to conduct basic research on the passive telemetry sensing mechanism and high temperature sensitive materials in order to develop a novel passive wireless sensor to be used for high temperature rotating component monitoring. Particularly, the proposed project aims to accomplish:

(1) An innovative *RF* powered telemetry sensor scheme development;

(2) High temperature sensitive material exploration and validation;

(3) Wireless capacitive sensor design and simulation;

(4) Sensor performance investigation and optimization;

(5) Sensor prototype fabrication and high temperature calibration.

1.5 Thesis Organization

The thesis consists of eight Chapters. Chapter 2 is a review of the state-of-the-art high temperature sensing technology. Chapter 3 presents the design of a novel wireless temperature sensor composed of planar capacitors and inductors, followed by a discussion on design principle and the electric modeling. In Chapter 4, high temperature sensitive material preparation and the validation of its operation in harsh environments is investigated. Chapter 5 covers a sensor performance analysis with respect to resonant frequency, quality factor, coupling factor and many others. Furthermore, several measurements are also proposed to enhance the sensor performance. In Chapter 6, sensor prototype fabrication and *LTCC* sensor packaging introduction based on Green Tape are discussed. In addition, sensor calibration is given during temperature range from 20 °C to 235°C. Finally, Chapter 7 summarizes the contributions of the work and the future improvements of the sensor technology.

2 Literature Review

Generally, temperature sensors involve the application of certain calibrated transducers converting a measurable quantity into a temperature value, such as electromotive force (thermocouples), radiated energy or volumetric expansion (thermometers), or some other characteristics of a material that varies reproducibly with temperature [15-21]. High temperature instruments (over 200 °C) having potential to work in harsh environments are reviewed briefly in this Chapter. These include high temperature thermocouples, high temperature optical sensors, high temperature *SAW* sensors and *RF* powered *LC* sensors.

2.1 High Temperature Thermocouples

A thermocouple is an assembly of two wires of different metals joined at one end, for temperature measuring, and at the other end, the cold junction, that usually works as a reference at 0°C. The open circuit voltage from these two wires, generated by an electromotive force inside the wires, depends on the difference in temperature between the hot and the cold junctions as well as the Seebeck coefficient of the two wire metals. Through the known cold junction temperature, the temperature of the hot junction can be obtained from the measured Seeback voltage. Different types of thermocouples are characterized to measure temperature up to certain levels with different resolutions [16]. Some available commercial high temperature thermocouples can even monitor temperature up to 2300°C.

However, the output from a thermocouple is a small signal can easily be affected by any common mode noises. Moreover, in chemically corrosive environments, high temperature thermocouples have a limited life of only a few days because of their

susceptibility to attack from corrosive chemicals. They drift significantly under high temperature environments during long-term operation.

2.2 High Temperature Optical Sensors

Optical sensors convert external physical stimulus such as temperature, pressure, strain, to optical signals. The optical beam is characterized by several variables, such as intensity, spectrum, phase and state of polarization. Many different physical phenomena related to these characteristics are used to perform sensing functions. For high temperature applications, the main existing techniques for optical thermometry are remote pyrometers (or radiation thermometers) [22-23], thermal expansion thermometers [24-25], fluorescence thermometers [26-28] and thermometers based on temperature dependent optical scatterings [29-30].

Remote pyrometers measure temperatures (up to 800°C) by detecting the thermal radiation emitted by the object. Thermal expansion thermometers are used to measure the change in optical path length of a short piece of material whose thermal expansion coefficient and refractive index change as a function of temperature and can be used in environment up to 1500 °C. Fluorescence thermometers can measure temperature up to 450 °C by detecting the decay time or intensity of a *UV* stimulated visible fluorescence pulse, which is temperature dependent.

Optical sensors are well developed technologies offering several significant advantages, such as small size, light weight, immunity to electromagnetic interference, and low cost. However, the performances attainable by these conventional techniques concerning measurement sensitivity, accuracy and range are limited in harsh environments.

2.3 High Temperature *SAW* Sensors

Surface Acoustic Wave *(SAW)* sensors have been applied widely for testing temperature, pressure, force, electric voltage, humidity or chemicals in gases [31-36]. Temperature *SAW* sensors, like most of them, are based on detecting the change in the phase velocity of the surface acoustic wave. As the acoustic wave propagates through or on the surface of the material, any changes to the characteristics of the propagation path affect the velocity and/or amplitude of the wave. Changes in velocity can be monitored by measuring the frequency or phase characteristics of the sensor and can then be correlated to the corresponding temperature quantity being measured. In fact, all acoustic wave sensors are piezoelectric acoustic wave sensors, which apply an oscillating electric field to create a mechanical wave, which propagates through the substrate and is then converted back to an electric field for measurement.

This technology is especially useful for harsh environment applications, where it is difficult to insert probes for measuring temperature due to low thermal mass, low conductivity of gases, and the strong radiation coupling of the components at high temperatures. However, the main difficulty with this technique is that the speed of sound is strongly dependent on not only temperature, but also environmental, geometric and material properties along the path, which is usually changed in different environmental conditions. Therefore, the effects yield low system capacity, low bandwidth and limit the range of application.

2.4 *RF* Powered *LC* Sensors

"Virtual batteries" powered by *RF* radiation is a promising alternative to chemical batteries. Because a battery is usually the element that limits the sensor lifetime and the operating temperature range, the wireless interrogation and remote powering achieved through an inductively powered system which generates a time varying electromagnetic field based on Faraday's law of induction and Lenz's law, has quite a potential. Initially and extensively used in private and security systems to transmit the data, *RF* powering has also been used to supply power and read data in the biomedical field. This method is particularly suitable for transmitting high energy for short distances as required in harsh medical and industrial environments, where, for example, the remote module is surrounded by metal. This low frequency range generally allows the use of higher data transfer rates, which is required for reading fast sensor response or reading multiple sensor modules [37].

The *RF* powered *LC* sensors are capable to eliminate the need for onboard power and exposed interconnections. Moreover, the small size and stable characterization make it use popular in various harsh environment measurement applications, such as pressure sensors [38-40], chemical sensors [41], and humidity sensors [42], etc.

In this thesis a *RF* powered *LC* temperature sensor will be developed. This sensor employs the sandwich multi-player piezoelectric films as well as electrodes to form an inductor capacitor (*LC*) resonator circuit. This resonant wireless platform removes any electronic components or physical contacts.

2.5 Conclusions

The majority of commercially available high temperature sensors are actually made using only a few basic types of instruments: liquid-in-glass thermometers, thermocouples and thermometers. As matured technologies having been used for several decades, they are inexpensive and their defects of systematic errors, instability or drift, are well understood. However, those commonly used traditional techniques are difficult to apply for measurements in hostile environments, e.g., electromagnetic interference, radiation, corrosion and rotating components. The measuring instruments should reduce the affect caused by the measurement environment and the use of wireless passive sensors is preferred.

Due to its immunity to electronics, compact size, a contact-less power supply, wireless data communication, resistance in high temperature rotating component monitoring and low cost, *RF* powered *LC* sensing technology will be chosen in this research project to develop a high temperature sensor capable of working in harsh environment.

3 Sensor Design and Simulation

This chapter starts with the design principle of the proposed temperature sensor. In this sensor, the energy transfer of the resonant circuit is based on the interaction between the inductor in the sensor and the reader antenna. Modeling and calculations of the planar capacitor and inductor are also discussed in order to determine the resonant frequency and temperature sensor range. Electrical modeling of the resonant circuit is built to simulate resonant frequency variations in response to temperature.

3.1 Design Principle

The temperature sensor, as shown in Figure 3.1, is composed of a ceramic multi-layer capacitor integrated with planar inductor, which forms an *LC* resonant circuit. This structural design makes the sensor easy to attach and can be used on round rotating components, like bearings in the aircraft engine.

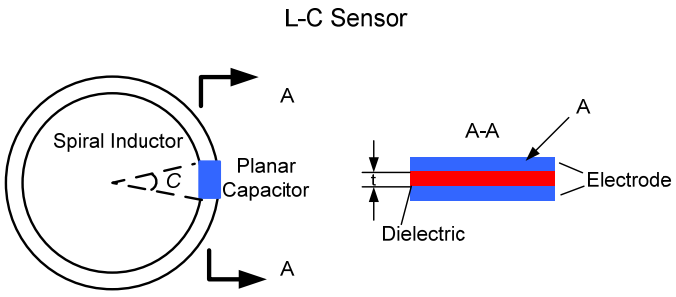

Figure 3.1 Schematic Diagram of Temperature Sensor

The design principle of this temperature sensor is based on electrical capacitance (*EC*). The capacitance of the sensor is a function of the dielectric constant of the sensitive

material. The planar capacitor, when exposed to harsh environments, has a linear dielectric constant variation with the temperature.

Figure 1.2 illustrates the power delivery and wireless data communication of the *LC* temperature sensor .The sensor itself does not have a power source or any transceiver circuits usually composed of electronics. It is powered by a remote reader which sends out an oscillating magnetic field across reader antenna by inductive link between the reader's antenna and the sensor's inductor. At the same time, the capacitance of the sensor changes in response to environmental variables - temperature. This provides the reader with a resonant frequency variation across the inductive link, by monitoring the impedance across the terminals of the wide bandwidth reader antenna.

3.2 Planar Capacitor

The planar capacitor, as shown in Figure 3.1 stores separated electric charges, and therefore energy. Equation 3-1 shows that charge *Q* stored is proportional to the voltage drop (across the capacitor):

$$Q=C\ V. \qquad \textbf{3-1}$$

The multi-layer planar capacitor consists of a dielectric substrate sandwiched between two parallel electrode plates. In general, the capacitance of a parallel-plate capacitor depends only on the dielectric constant and the geometry of the capacitor. Thus the energy of a charge configuration is dependent upon the relative permittivity and the separation distances.

The concept of the capacitive element of the sensor requires a change in the capacitance as a function of temperature. This would be fulfilled if the dielectric constant of the material between the plates of the capacitor changes along with the temperature. This

relationship between the dielectric constant and temperature is used to model the capacitive element of the temperature sensor, which can be expressed by equation 3-2:

$$C_S(T) = \frac{\varepsilon_0 \varepsilon_r(T) A}{t}. \qquad \textbf{3-2}$$

Here ε_0 is the permittivity of free space, $\varepsilon_r(T)$ is the relative dielectric constant of the dielectric material, sensitive to environmental temperature, A is the area of the electrode plate, and t is the distance between the electrodes, which is also the thickness of dielectric material.

Considering a possible sensor designs, where the thickness of the sensing material, t, is $0.480mm$ and its sensing area, A, varies from 10 mm^2 to 30 mm^2, in addition to having a dielectric constant that ranges from 500 to 5000. Based on this capacitive element concept, the relationship between capacitance and dielectric constant is illustrated in Figure 3.2.

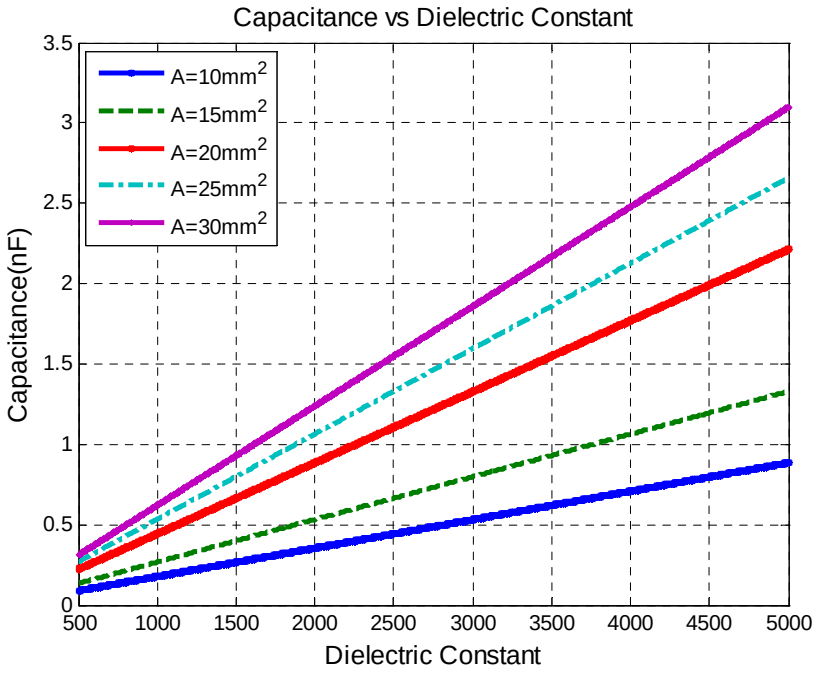

Figure 3.2 Capacitance *vs.* Dielectric Constant

3.3 Spiral Inductor

Spiral inductors (Figure 3.3) are utilized widely to make resonant circuit elements for capacitive sensors in the microelectronics field. They provide high quality factor elements and are feasible in harsh environment applications.

Coupling the primary reader antenna, as illustrated in Figure 1.2, the spiral inductor acts as a transformer based on the principle of electromagnetic induction. When an oscillating current is executed on the antenna, a changing magnetic field to both the primary antenna and the spiral inductor is produced along the magnetic path in the air. An alternating voltage of the same frequency is induced in the spiral inductor. The environmental temperature variations induce the frequency change, which can be detected from reader side by monitoring the impedance across the terminals of the wide bandwidth reader antenna. In other words, the electrical energy is transferred from the input antenna to the sensor and the temperature information can be detected by the reader from the coupled magnetic field.

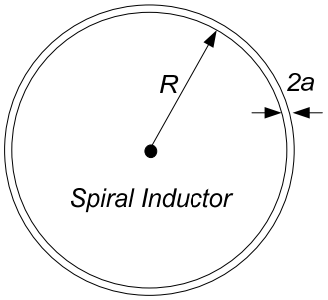

Figure 3.3 Schematic View of Spiral Inductor

In order to read out the temperature information, it is necessary to design and fabricate an appropriate spiral inductor to have both a reasonable inductance and quality

factor at high temperatures. Inductance (or electric inductance) is a measurement of the amount of magnetic flux produced for a given electric current. Strictly speaking, this quantity is called self-inductance, because the magnetic field is created solely by the conductor that carries the current. The self-inductance of a straight conductor of length, *l,* and radius, *a,* (neglecting the effects of nearby conductors), is given by [43]:

$$L \approx \frac{\mu_0 l}{2\pi}\left[\ln\left(\frac{2l}{a}\right) - 0.75\right]. \qquad \textbf{3-3}$$

Here the magnetic permeability of free space, μ_0, is $4\pi \times 10^{-7}$ H/m. Different types of spiral inductors have respective calculation equations according to [44]. However, there is no closed-form solution for the inductance of circular loops. The self-inductance of a circular loop of round wire, as shown in Figure 3.3 has a low frequency inductance that can be estimated according to equation 3-4 [43]:

$$L \approx n^2 \mu_0 R\left[\ln\left(\frac{8R}{a}\right) - 1.75\right]. \qquad \textbf{3-4}$$

Here the loop radius is *R,* the wire radius is *a,* and *n* corresponds to the turns of the inductor. Figure 3.4 indicates how the coil turn and inductor radius affect inductance, for a wire radius *a* of 0.337mm.

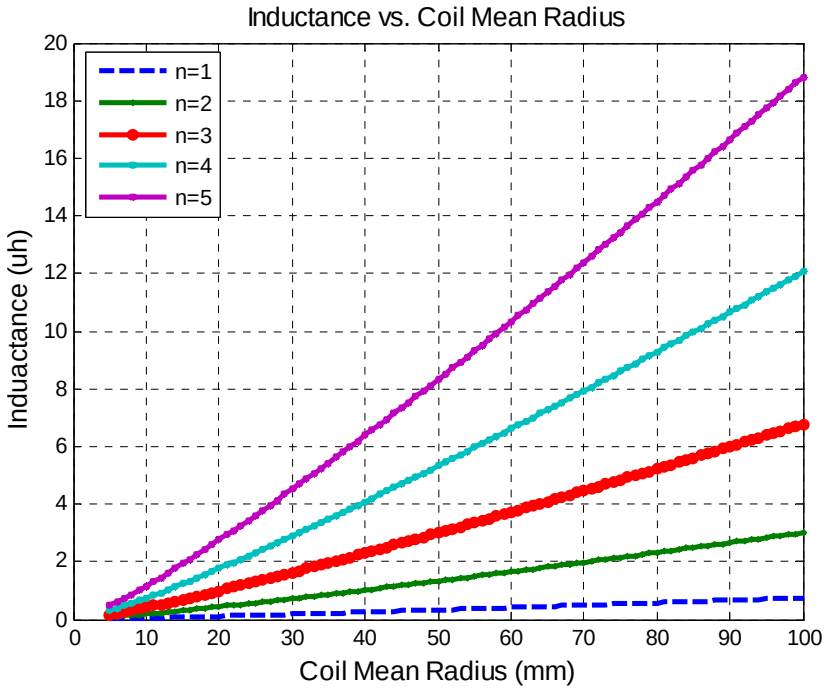

Figure 3.4 Inductance *vs.* Coil Mean Radius

3.4 Electrical Model of Resonant Circuit

The multi-layer ceramic structure developed has an integrated passive resonant circuit consisting of a spiral inductor and a parallel-plate capacitor. The inductance of the resonant circuit is fixed and the capacitance varies as a function of temperature. Therefore, the resonant frequency of the circuit changes in response to temperature. Ultimately, the relationship between resonant frequency and temperature is used to determine the measured temperature wirelessly.

The sensor's theoretical electrical model as well as the reader coil used for inductive powering is illustrated by a parallel palate capacitor, C_S, and spiral inductor, L_S, as shown in Figure 3.5. In this Figure, R_R is the resistance existing in the reader side and R_S is the

resistance in the sensor circuit. A time variant current, $I_{1,}$ enables the resonant frequency to vary in time with a given interval, T; C_R is the capacitance of the reader circuit that is used to maximize the current applied through the reader antenna; and M is the mutual inductance. The frequency of this current, $\omega,$ is a linear function with respect to time and can be given by:

$$\omega = \Delta\omega \cdot t + \omega_0 (T \le t \le T + \Delta t) . \qquad \textbf{3-5}$$

Once a current of varying frequency is applied to the primary coil (the antenna of the reader), a varying magnetic field is generated around this coil. Based on Faraday's law, induced voltage is generated on the remotely placed inductor of the sensor.

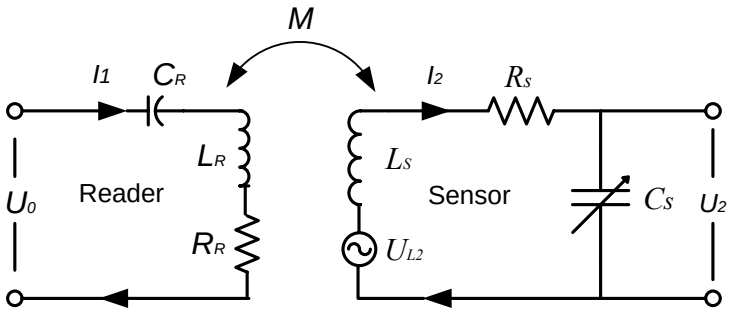

Figure 3.5 Inductively Coupled Circuit

If U_{L2} indicates the voltage induced in the sensor inductor, it can be calculated by equation 3-6:

$$U_{L2} = j\omega M I_1 . \qquad \textbf{3-6}$$

The voltage U_2 on the capacitor of the sensor can be expressed as follows [45]:

$$U_2 = U_{L2} - j\omega L_S I_2 - R_S I_2 . \quad \textbf{3-7}$$

And the current is determined by equation 3-8:

$$I_2 = j\omega C_S U_2 . \quad \textbf{3-8}$$

Therefore, by solving Equation 3-7 and 3-8, the voltage across the planar capacitor U_2 becomes

$$U_2 = \frac{U_{L2}}{1 + \left(j\omega L_S + R_S\right) \cdot j\omega C_S} . \quad \textbf{3-9}$$

When this planar resonance sensor is placed in the time-variant magnetic field of the reader antenna L_R, the voltage U_{L2} will be induced between the inductor of the sensor. Once the capacitance of the sensor changed according to environment temperature, U_2 will change accordingly and then a change is detected in the voltage U_0 across the reader.

This means that the capacitance change at a certain frequency is measured as variation of voltage. However, this change in voltage U_0 is too insignificantly small to measure. Since the capacitance variation will change the resonant frequency (f_r) of the planar resonator, usually a signal is used to generate a periodical sweep in frequency around the sensor's natural frequency to measure the frequency variation, instead of measuring the

voltage variation at a certain frequency. Therefore, the frequency response of U_0 on the reader coil is measured to monitor the impedance change due to the temperature-dependent capacitance (C_s) variation on the sensor. In this way, a very small variation in the impedance can be measured.

The voltage response of the reader's antenna coil verses sweep frequency without the present of a sensor can be calculated by

$$U_0 = \left(j\omega L_R + R_R \right) \cdot I_1 . \qquad \textbf{3-10}$$

And the voltage response of the reader's antenna coil verses sweep frequency with the present of a sensor can be calculated by

$$U_0 = \left(j\omega L_R + R_R + \frac{\omega^2 k^2 L_R L_S}{j\omega L_S + R_S + \frac{1}{j\omega C_S}} \right) \cdot I_1 . \qquad \textbf{3-11}$$

The coefficient k given in equation 3-12 is defined by:

$$k = \frac{M}{\sqrt{L_R L_S}} . \qquad \textbf{3-12}$$

The resonant frequency of the sensor indicates the point where the voltage appears as an abrupt change. Generally speaking, the resonant frequency occurs at the peak of the

voltage plot during a sweep frequency range. The expression of the resonant frequency is defined by the following equation:

$$f_r = \frac{1}{2\pi\sqrt{L_s C_s}}. \qquad \textbf{3-13}$$

Here L_S and C_S were defined according to equation 3-2 and 3-4 respectively.

In order to record the information of temperature variation, the resonant frequency should be within a range detectable by a reader. Figure 3.6 indicates the relationship between resonant frequency and dielectric constant, based on the capacitance and inductance simulation. In this plot, parameters are used for a group of sensing area, *A,* ranging from *10* mm^2 to *30* mm^2, a thickness of the sensitive material, *t,* of *0.480 mm,* a wire radius, *a,* of *0.337mm,* an inductor radius, *R,* of *8.5mm,* and the turns of the inductor, *n,* of *2.*

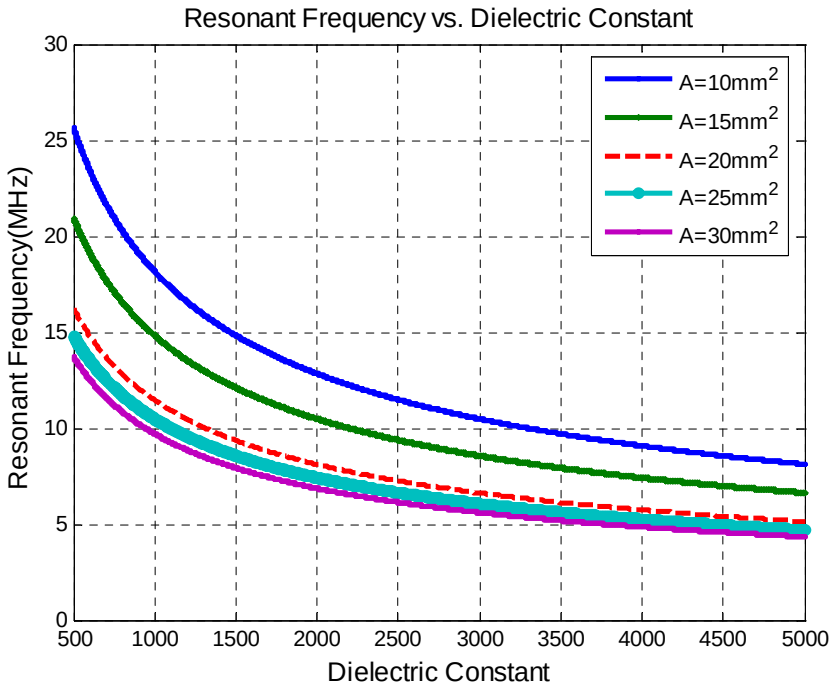

Figure 3.6 Resonant Frequency *vs.* Dielectric Constant

3.5 Conclusions

In this chapter, design principle of the passive capacitive temperature sensor and electrical model of the resonant circuit are presented. The energy transfer mechanism is demonstrated, which is based on the interaction between the inductor on the sensor and the coil antenna on the reader. Electrical model of resonant circuit is built to simulate resonant frequency variations in response to temperature. In order to locate the resonant frequency within detectable range, modeling with respect to the geometric dimensions of the planar capacitor and inductor are built. The sensor prototype was fabricated based on these design considerations. The spiral inductor with two turns was made of copper wire leads, connected to the electrodes of the capacitor using *6041D* Ag paste. The diameter of the round copper wire was *0.674 mm* and the radius of the inductor was *28.5 mm.* The area of the electrode plate was $25mm^2$ and the thickness of dielectric material was *0.480 mm*.

4 High Temperature Sensitive Materials

This Chapter conducts the exploration and validation of high temperature sensitive materials. High temperature ceramic materials and piezoelectric materials are discussed and compared in order to select material candidates with good temperature sensitivity, excellent electrical properties capable of high temperature applications.

4.1 High Temperature Ceramic Materials

Dielectric ceramics are electrical insulators with dielectric strength, dielectric constant and loss tangent values tailored for specific device or circuit applications. Generally, the dielectric constant is used to determine the ability of an insulator to store electricity energy. When a material is utilized in electric application where the high capacitance is needed, a high dielectric constant is required to increase the charge that can be stored. High temperature applications, combined with higher density interconnections demand the use of materials that provide adequate thermal management, excellent thermal stability and heat dissipation. These ceramic materials also require have high thermal conductivity, low thermal expansion, good electrical insulation, corrosion-resistance and stability in harsh environments. The following sections will provide some commonly used commercial ceramic materials, including Beryllium Oxide (*BeO*), Aluminum Nitride (*AlN*), Alumina (Al_2O_3) and Macor. The main mechanical properties of the aforementioned materials are provided in Table 4-1, according to [46-47].

Table 4-1 Mechanical Properties Comparison (25ºC, 1 kHz)

Property	AlN	BeO	Al_2O_3	Macor
Dielectric constant	8.9	6.7	9.8	6.03
Dielectric loss	0.0001	0.0003	0.0002	0.0047
Resistivity (Ohm-cm)	$>10^{14}$	$>10^{14}$	$>10^{14}$	$>10^{16}$
Thermal conductivity (W/mK)	170-200	260	36	2.63
CTE (ppm/C)	4.6	8.5	8.2	
Density (g/cm^3)	3.30	3.85	2.89	2.52
Bending strength (MPa)	290	230	380	
Hardness (GPa)	11.8	9.8	14.1	
Young's mod (GPa)	331	345	372	66

4.1.1 Beryllium Oxide (BeO)

Many applications exploit beryllium oxide (*BeO*)'s excellent electrical insulating properties, high mechanical strength, high thermal conductivity as well as good dielectric properties. As shown in Figure 4.1, *BeO*'s dielectric constant varies from 6.4 to 9.0 in a temperature rang from 150 °C to 420 °C, according to experimental record, measured in 1 kHz [48]. It is particularly well suited as a heat sink and heat dissipation medium in integrated circuitry. But there is one thing we have to mention, beryllium oxide powders are toxic when inhaled or ingested. The cost of *BeO* is expensive. For example, one price of commercial *BeO* of *25mm x 25mm x 1.5 mm* size will cost more than $ 300.00 [49].

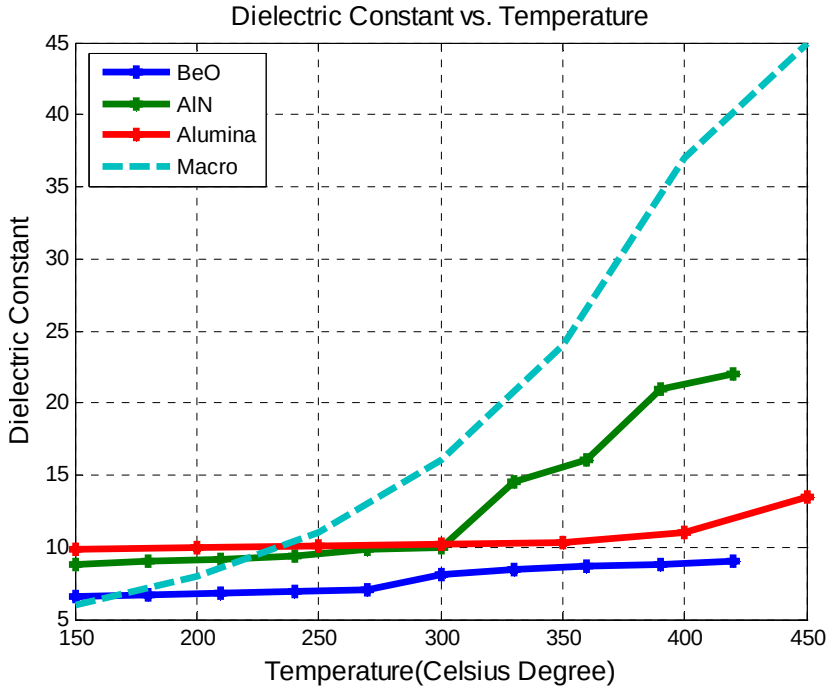

Figure 4.1 Dielectric Constant Variation Comaprison

4.1.2 Aluminum Nitride

Aluminum nitride *(AlN)* is typically applied in telecommunication, optoelectronics, automotive and military applications requiring high thermal dissipation, high volume capabilities, high reliability in harsh environments and consistent performance. According to experiment record measured at 1 kHz [48], its dielectric constant changes from 8.7 to 22.0 in a temperature range from 150 °C to 420 °C, as shown in Figure 4.1. Its high thermal conductivity and better heat dissipation simplify thermal design and significantly improves circuit life and reliability. Aluminum nitride substrates have long been known to be safer to handle and have lower cost than beryllium oxide (*BeO*). The main drawback of *AlN* is its potential reactivity with water vapor in high temperature, moist environments.

4.1.3 Alumina

Alumina or Aluminum Oxide (Al_2O_3) is another high temperature ceramic material candidate. As shown in Figure 4.1, its dielectric constant has a large change from 10.0 to 40.0 during a temperature range from 150 °C to 650 °C, which is measured at 10 kHz [50]. Although its thermal conductivity is not as high as *BeO*, its high volume resistivity, chemical stability in aggressive and high temperature environments, along with its high dielectric constant coupled with low dielectric loss and excellent electrical insulation lead to its wide applications in electronics as substrates. Moreover, its cost is much lower than *BeO*.

4.1.4 Macor

Macor has very good temperature dependent dielectric changes from 6.7 to 40.0 in the range from 100 ºC to 450 ºC at 1 kHz [51], as illustrated in Figure 4.1. Macor is an outstanding engineering material, having a continuous use temperature of 800ºC and a peak temperature of 1000 ºC. Its fabrication is easy and fast because it can be machined into complicated shapes and precision parts with ordinary metal working tools, quickly and inexpensively, and it requires no post firing after machining. That means no frustrating delays, no expensive hardware, no post fabrication shrinkage, and no costly diamond tools to meet specifications.

4.2 Piezoelectric Materials

Piezoelectric materials are historically utilized widely for strain gages, accelerometers and sonar based on direct piezoelectric effect and converse piezoelectric effect. In the direct piezoelectric effect, the application of a mechanical load on the piezoelectric materials induces an electric response, and vice verse in converse piezoelectric effect. However,

another characteristic behavior of piezoelectric materials is the pyroelectric effect, in which the piezoelectric material responds to changes in temperature by producing an electrical response, which will influence the dielectric constant variation in changing temperature environments. Piezoelectric materials based on high-k ceramic dielectrics offer the best pyroelectric effect, high sensitiveness and provide large and stable temperature dependent dielectric constant changes. In addition, devices made from high-k dielectric ceramics are more compact, which makes it then feasible for harsh environment applications. Actually, most high-k dielectric ceramics are ferroelectric in nature. In the following section, we will discuss the properties and comparisons of several ferroelectric materials.

4.2.1 Ferroelectricity

Ferroelectricity is a phenomenon which was discovered in 1921. The name refers to certain magnetic analogies. It has also been called Seignette electricity, as Seignette or Rochelle Salt (*RS*) was the first material found to show ferroelectric properties such as a spontaneous polarization on cooling below the Curie point, ferroelectric domains and a ferroelectric hysteresis loop. A huge leap in ferroelectric material research began in the 1950's, leading to the widespread use of barium titanate (*BaTiO3*) based ceramics in capacitor applications and piezoelectric transducer devices. Since then, many other ferroelectric ceramics including lead titanate (*PbTiO3*), lead zirconate titanate (*PZT*), lead lanthanum zirconate titanate (*PLZT*), and relaxor ferroelectrics like lead magnesium niobate (*PMN*) have been developed and utilized in a variety of applications [52-54]. With the development of ceramic processing and thin film technology, many new applications have emerged. The biggest use of ferroelectric ceramics have been in the areas of dielectric ceramics for capacitor applications, ferroelectric thin films for non volatile memories,

piezoelectric materials for medical ultrasound imaging and actuators, and electro-optic materials for data storage and displays[55-59]. Furthermore, ferroelectric materials can potentially operate over a wide temperature range reaching as low as –270 °C to as high as +650 °C. Single crystals, like *LiNbO3*, have a Curie temperature higher than 1000 °C.

In order to investigate the feasibility of producing sensors that can operate under high temperature, metal surrounded rotating environments; the properties of a series of ferroelectric materials were studied. These piezoelectric materials were examined because they are solid state and can be designed as sensors to withstand high stroke, high speed and high stability. The data for dielectric constant analysis as a function of the temperature, based on experiments or commercial data sheets, will be presented.

The temperature dependence of the dielectric constant obeys the well known Curie-Weiss law and is given in equation 4-1:

$$\varepsilon_r = \frac{C}{T - T_c}. \qquad \textbf{4-1}$$

Here ε_r corresponds to the relative magnetic susceptibility, C indicates a material-specific Curie constant. T is the absolute temperature and T_c is the Curie temperature, measured in degrees Kelvin. Since the permittivity (dielectric constant) peaks of ferroelectric materials lie at their Curie point T_c, and the loss increases dramatically after Curie point, it would be most efficient to integrate dielectric ceramics for temperature monitoring below the Curie temperature T_c [60].

Following is a quick discussion of several possible ferroelectric materials that could be used in our proposed temperature sensor application.

4.2.2 Lead Zirconate Titanate (PZT)

The dielectric constant (permittivity) of the *PZT* thin film has a big variation from 420 to 540 in a temperature range from 200 °C to 440 °C, which was measured at 10 kHz [61] , as shown in Figure 4.2. The permittivity maximum is found at 375 ºC, close to the Curie temperature, 380 ºC, of *PZT* in the morphotropic phase boundary composition, where the *Zr/Ti* relative concentration is *53/47*. Below the transition temperature T_c, the dielectric constant increases quickly with temperature. Above T_c, values start to fall but increase again after further heating. This behavior can be explained by the presence of other ferroelectric phases with higher transition temperature, like the behavior found in $PbTiO_3$.

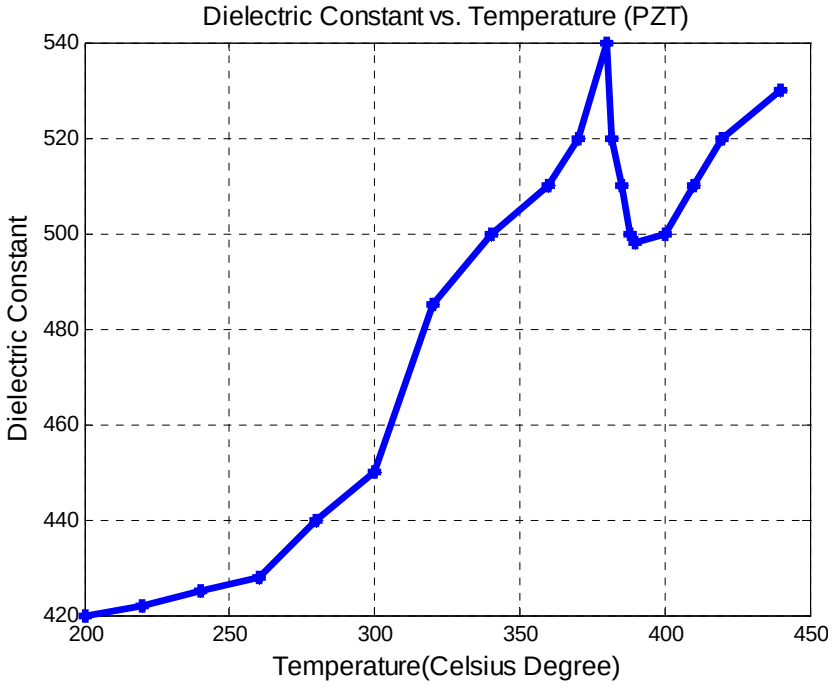

Figure 4.2 Dielectric Constant *vs.* Temperature of *PZT*

4.2.3 Lead Lanthanum Zirconate Titanate (PLZT)

PLZT is a transparent ferroelectric ceramic formed by doping La^{3+} ions on the A sites of (*PZT*). The electric applications of *PLZT* ceramics depends on the composition. Figure 4.3 shows the dielectric properties of ceramic powders *PLZT* 10/65/35, as a function of temperature, based on experimental results in [62], which is measured in 1 kHz. This transparent *PLZT* ferroelectric ceramic is produced by combining the chemical method developed by Menegazzo and Eiras [63] and uniaxial hot-pressing.

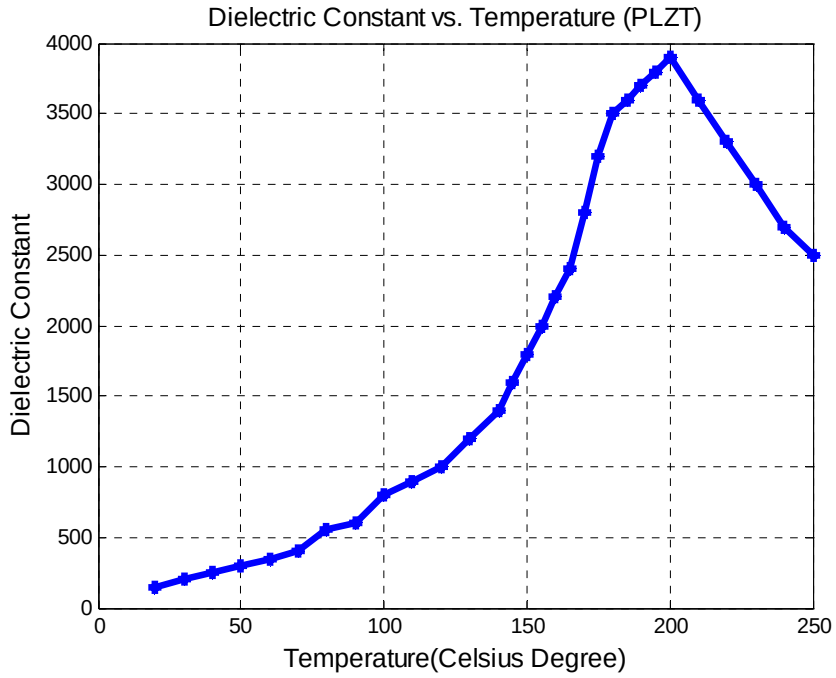

Figure 4.3 Dielectric Constant *vs.* Temperature of *PLZT*

4.2.4 Lead Nb Zirconate Titanate (PNZT)

Niobium modified lead zirconate titanate (*PNZT*) materials are formed by adding *Nb* to a *PZT* composition. The *Nb* addition enhances domain reorientation resulting in square

hysteresis loops, higher coupling factors and reduced aging. The dielectric constant variation as a function of temperature is shown in Figure 4.4 [64].

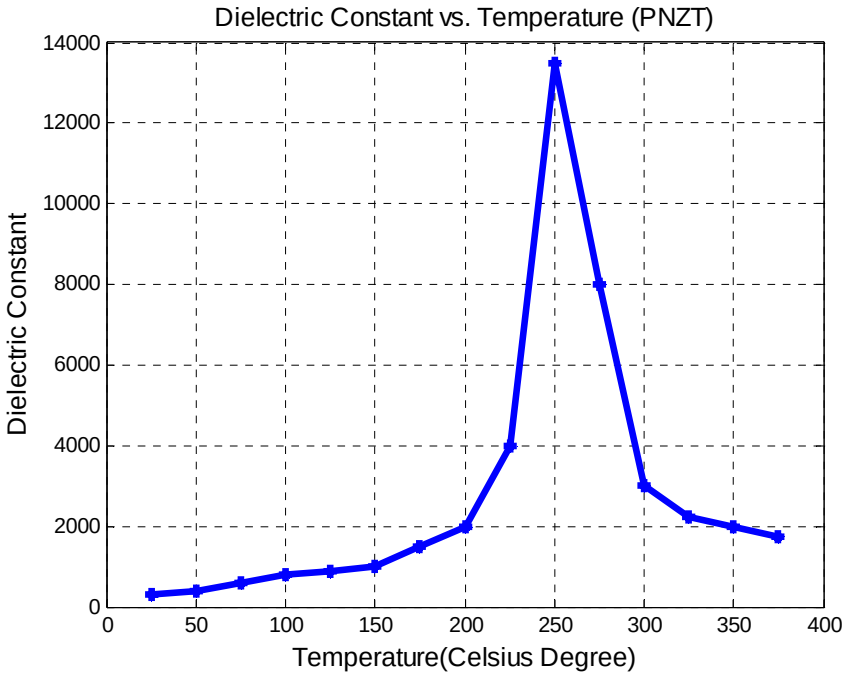

Figure 4.4 Dielectric Constant *vs.* Temperature of *PNZT*

4.2.5 Lead Bi Lanthanum ZirconateTtitanate (PLBZT):

Polycrystalline samples of bismuth *(Bi)* doped lead lanthanum zirconate titanate (*PLZT*) near the morphotropic phase boundary *(MPB)* were synthesized by a solid solution mixing technique in [65]. The dielectric constant behavior of four different types of *PLBZT* is shown as a function of temperature ranging from room temperature to 600 Kelvin, at 10 kHz, as illustrated in Figure 4.5.

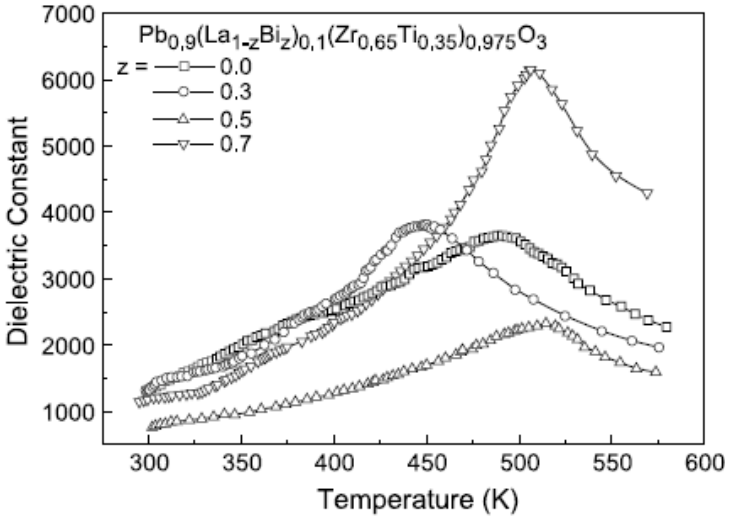

Figure 4.5 Dielectric Constant *vs.* Temperature of *PLBZT*

4.3 Conclusions

This Chapter discusses the potential dielectric materials for high temperature applications. Comparing high temperature ceramic materials, Alumina has better thermal conductivity, excellent electrical insulation and low cost, no toxic powder. However, experiments indicate that the capacitance variation is insensitive with temperature variation. Especially in temperatures less than 350 °C, the dielectric constant is almost constant. But Alumina is a good candidate as the substrate of the sensor. Later on, we selected commercial Alumina ---Dupont Green Tape ™ as sensor substrate.

According to the Curie-Weiss law, a preferred material is the one that displays the largest change in dielectric constant with temperature, which can be expressed by:

$$\frac{d\varepsilon_r}{dt} = \frac{-C}{(T - T_c)^2}. \qquad \textbf{4-2}$$

Thus at a given temperature, the material with the largest dielectric constant temperature dependence is the material with the largest Curie constant, *C*. In addition, the material with the largest Curie constant will also display the largest peak dielectric constant value. Thus, by comparing peak dielectric constant values as well as Curie temperature in the literature, a commercial material of *PLZT* is selected as high temperature sensitive material candidate for the sensor that will be developed. The sensor prototype processing based on this commercial material will be introduced in Chapter 6.

5 SENSOR PERFORMANCE ANALYSIS

In order to obtain an optimal sensor configuration with high sensitivity, high *Q*-factor, small size, long communication distance, sensor performance analysis will be investigated in this Chapter.

5.1 Modeling and Simulation

The temperature sensor that will be developed will be placed within the magnetic field induced by an alternating current, which is generated by the remote reader across inductive powering, as shown in Figure 5.1. In this resonant circuit, Z_R, and Z_S, are the reader and sensor inherent impedances respectively. R_R, and R_S, are the self resistances of the reader and the sensor circuit. The capacitance of the reader, C_R, is used to maximize the current applied through the reader antenna; C_S, is the sensor capacitance, which is sensitive to environment temperature. Z_s' is the reflected impedance of the sensor, and, M, is the mutual inductance.

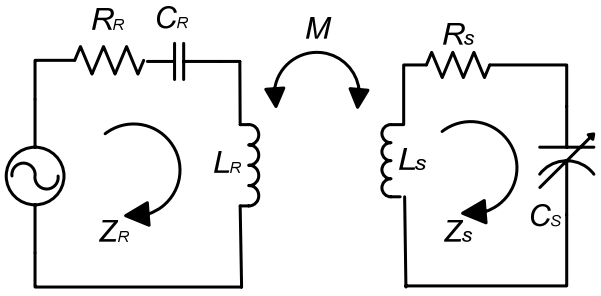

Figure 5.1 Inductive Coupled Reader and *LC* Sensor

Usually, the classical approach to analyze this resonant circuit is to eliminate the coupled reader coil and the sensor by reflecting impedances back to the reader, in order to clarify the voltage change of reader coil. The equivalent circuit diagram of the resonant circuit of the reader with the inductive coupled sensor is shown in Figure 5.2.

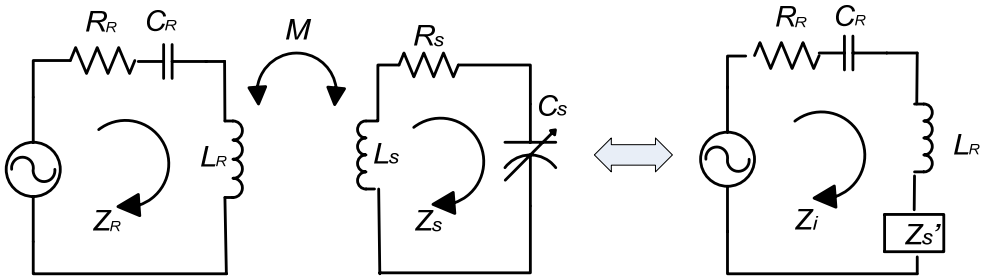

Figure 5.2 Equivalent Circuit Diagram of Wireless Telemetry System

The impedance of the resonant circuit of the reader is given by:

$$Z_R = j\omega L_R + R_R + \frac{1}{j\omega C_R}. \qquad \textbf{5-1}$$

In addition, the impedance of the sensor side can be expressed as:

$$Z'_S = \frac{(\omega M)^2}{j\omega L_S + R_S + \frac{1}{j\omega C_S}} = -\frac{\omega^2 k^2 L_R L_S}{j\omega L_S + R_S + \frac{1}{j\omega C_S}}. \qquad \textbf{5-2}$$

Here *k* is the coupling coefficient, defined by:

$$k = \frac{M}{\sqrt{L_R L_S}}. \qquad \textbf{5-3}$$

In fact, the sensor interaction can be seen as a load variation $\Delta Zs'$ placed in series with the inductance antenna, which can be expressed by:

$$\Delta Z_S' = \frac{\omega^2 k^2 L_R L_S}{j\omega L_S + R_S + \frac{1}{j\omega(C_S + \Delta C_S)}}. \qquad \textbf{5-4}$$

The input impedance seen from the reader side is given by

$$Z_i = Z_R + Z_S'. \qquad \textbf{5-5}$$

Substituting of equations 5-1 and 5-2 into 5-5, will yield:

$$Z_i = j\omega L_R + R_R + \frac{1}{j\omega C_R} + \frac{\omega^2 k^2 L_R L_S}{j\omega L_S + R_S + \frac{1}{j\omega(C_S + \Delta C_S)}}. \qquad \textbf{5-6}$$

Therefore, the input impedance seen from the reader is given by

$$Z_i = j\omega L_R + R_R + \frac{1}{j\omega C_R} + \frac{\omega^2 k^2 L_R L_S}{j\omega L_S + R_S + \frac{1}{j\omega(C_S + \Delta C_S)}} \quad \textbf{5-7}$$

A voltage drop caused by the sensor side circuit is equivalent to the reflected impedance Z_S' multiplied by the current. Actually, instead of measuring the voltage change at a certain frequency, a signal is used to generate a periodical sweep of the frequency around the sensor's natural frequency to measure a frequency variation. This reflected sensor impedance changes in response to sensor capacitance changes when the reader's frequency is swept. When the excitation frequency matches the sensor side resonant frequency, a sudden increase in the sensor impedance Z_S' occurs. Figure 5.3 shows the magnitude of impedance and phase of this reflected sensor impedance Z_S' in response to the sweeping frequency changes, with the parameter values summarized in Table 5.1.

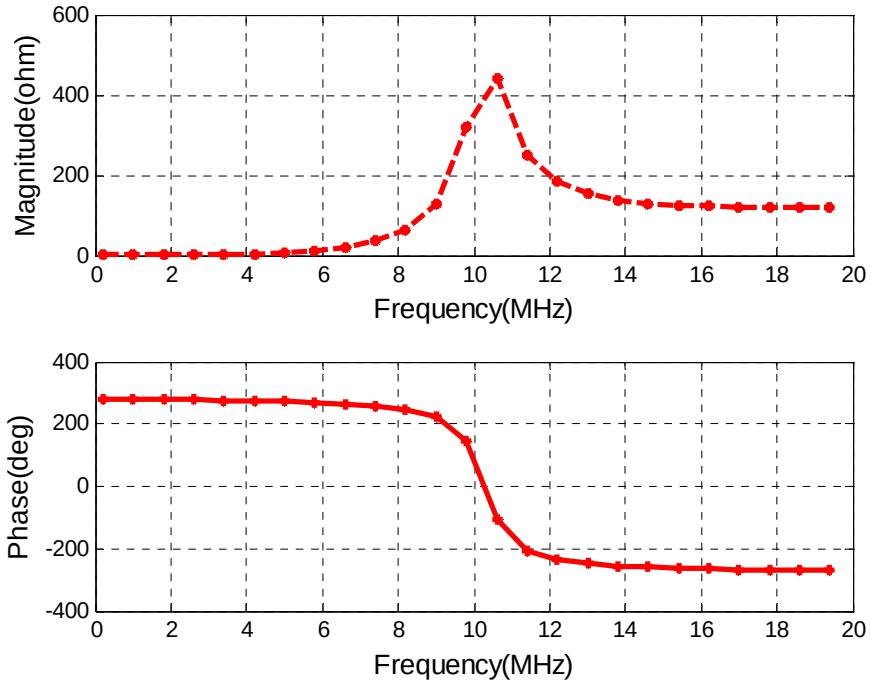

Figure 5.3 Magnitude & Phase Angle of Z_S'

When temperature increases or decreases, the dielectric constant will enhance or reduce, which induces the variation of sensor's capacitance, C_S, and then the input impedance Z_i. The impedance Z_i changes with respect to temperature are shown in Figure 5.4.

Table 5-1 System Parameter Values (at 20 ºC)

Reader Inductance L_R	1.5 μH
Sensor Inductance L_S	0.68 μH
Sensor Total Resistance R_L	6ohm
Sensor Nominal Capacitance C_S	0.24 nF
Nominal Coupling Factor k	0.4
Reader Radius r_R	30cm
Inductor Radius r_S	28.5cm
Coupling Distance d	2.5cm

When temperature increases, the peak of the input impedance Z_i will move toward to the left accordingly, this means that the resonant frequency will decrease as the temperature reduce. The curve shown in Figure 5.4 was simulated using the same parameter values shown in Table 5.1.

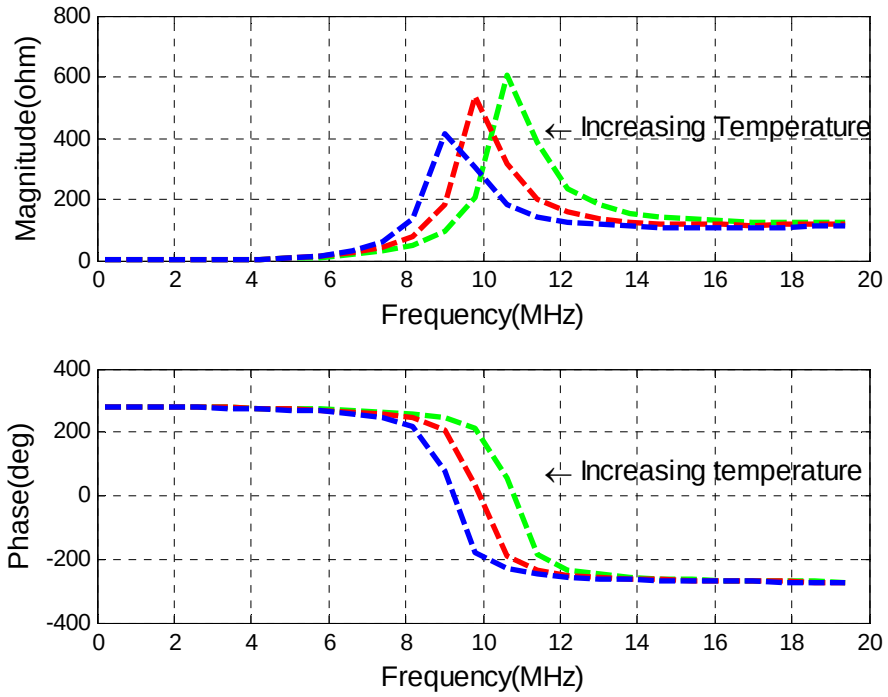

Figure 5.4 Resonant Frequency of Input Impedance *vs.* Temperature

5.2 Performance Analysis

Sensor performance will be analyzed in this section, involving resonant frequency, *Q*-factor, coupling distance and capacitance compensation.

5.2.1 Resonant Frequency

A general resonant circuit is comprised of elements that dissipate energy and store energy: resistive components dissipate energy and reactive components store energy. Stored energy gives rise to a phase shift between the voltages and currents in a system. It is customary to employ complex variables to describe such systems, such that a measured real quantity is in phase with the excitation signal and a measured imaginary value is 90 degrees out of phase with the excitation signal. A positive value of reactance is defined as inductive

and a negative value of reactance is defined as capacitive. Any passive circuit has the following properties at resonance:

(1) At resonance, inductive stored energy is equal to the capacitance stored energy. Since they are of opposite signs, the reactance cancels each other.

(2) Since the reactance vanishes at resonance, the observed impedance of the circuit is purely resistive. Mathematically, this implies that the measured impedance is thus purely real with zero phase shifts.

(3) Provided that the losses in the circuit are small relative to the reactance, the magnitude of the measured voltages and currents shall exhibit a pronounced peak (or dip) in the vicinity of resonance.

The expression of the resonant frequency is given by the following equation:

$$f_r = \frac{1}{2\pi\sqrt{L_s C_s}}. \qquad \textbf{5-8}$$

This resonant frequency is defined in terms of sensor electrical parameters and indicates the peak of magnitude and zero crossing point of the phase of the reflected sensor impedance, Z_S', as shown in Figure 5.3. In order to detect the resonant frequency from the reader's side, the reflected impedance, Zs', should be high enough. If the changes of reflected impedance from the sensor, Zs', are smaller than those of inductance from the antenna, most of the voltage drop will occur across the antenna. This will bury the change of reflected impedance, Zs', caused by the remote sensor. For that reason, the Q-factor and coupling coefficient should be high enough to make sure that the resonant frequency can be detected.

5.2.2 Q-factor

Resonance is a frequency-dependent stimulated response characterized by a large amplitude response at a specific frequency. This amplitude response is an indication that a resonant system has the ability to store energy at a particular resonant frequency. Energy storage in a passive material structure is sustained by a continuous exchange between one form of energy and another. This transfer of energy is sometimes called circulating power. Energy can be found in the form of kinetic energy and potential energy, or can be expressed in terms of electric fields and magnetic fields, currents and voltages, mechanical stresses and strains, pressure and displacement, or a mixture of these. The ratio of total stored energy to dissipated energy per unit cycle defines the quality factor, Q, of the resonator:

$$Q = \frac{W_{total}}{P/2\pi f} = \frac{2\pi f W_{total}}{P} \quad . \qquad \textbf{5-9}$$

Here, W means total stored energy, P is the average dissipated power, and f is the resonant frequency.

In order to exhibit a large amplitude response, low internal losses and weak coupling to the external environment are also required. A higher Q-factor indicates a lower rate of energy dissipation relative to the oscillation frequency. Generally, the Q-factor is interpreted as an indication of the sharpness of the resonance peak. The simplified expression of Q-factor is defined by:

$$Q = \frac{2\pi f_r L_S}{R_L} = \frac{1}{R_L}\sqrt{\frac{L_S}{C_S}} \quad . \qquad \textbf{5-10}$$

Here, R_L is the total sensor resistance consisting of the inductor resistance, capacitor resistance and circuit resistance, which is briefly discussed by Musunuri et al. in [66].

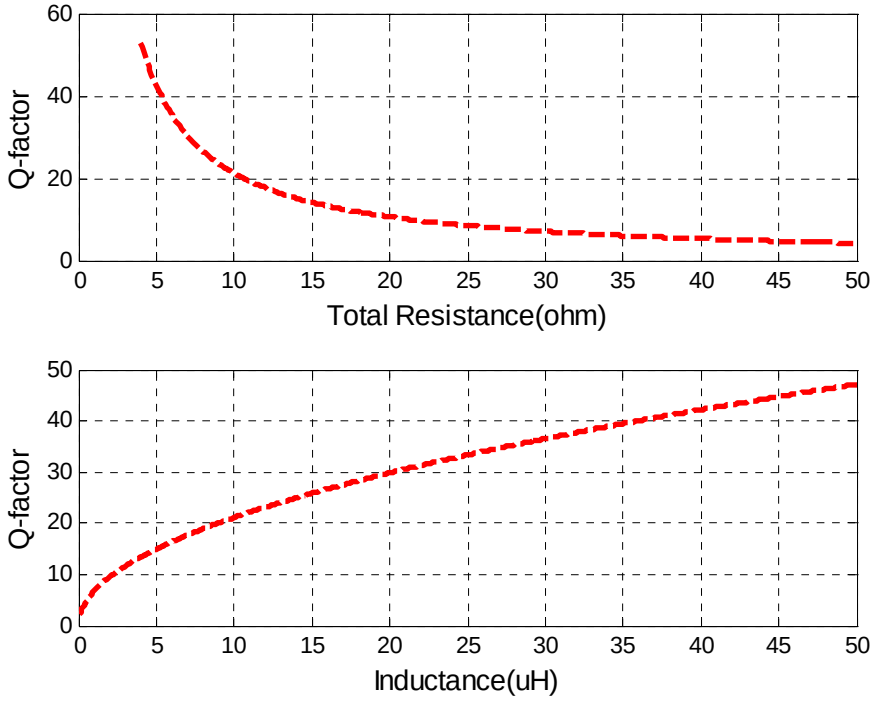

Figure 5.5 *Q*-factor *vs.* Resistance & Inductance

Figure 5.5 depicts the variation of the *Q*-factor with respect to total sensor resistance and sensor inductance for the same nominal value of other parameters as shown in Table 5.1. This simulation shows that minimizing the total resistance and maximizing sensor inductance will improve the *Q*-factor.

5.2.3 Coupling Factor

The coupling coefficient, *k,* is the dominate factor for the wireless range of inductive telemetry systems. For a complete system description, *k* can be modeled and optimized specifically for each application by using finite element, *CAD* tools and models. However, a fair approximation of *k* related to design parameters is given by:

$$k(d) = \left(\frac{r_S r_R}{d^2 + r^2}\right)^{\frac{3}{2}}. \qquad \textbf{5-11}$$

Here, r_R corresponds to the radius of the primary coil, r_S indicates the radius of the sensor inductor, and *d* is the coupling distance [67].

Figure 5.6 illustrates how the reader antenna radius and the radius ratio of the sensor radius and the reader antenna affect the coupling factor, *k*, at a certain communication distance shown in Table 5.1. The plot indicates that minimizing the antenna radius and maximizing the radius ratio will improve the coupling factor and maximize the coupling distance.

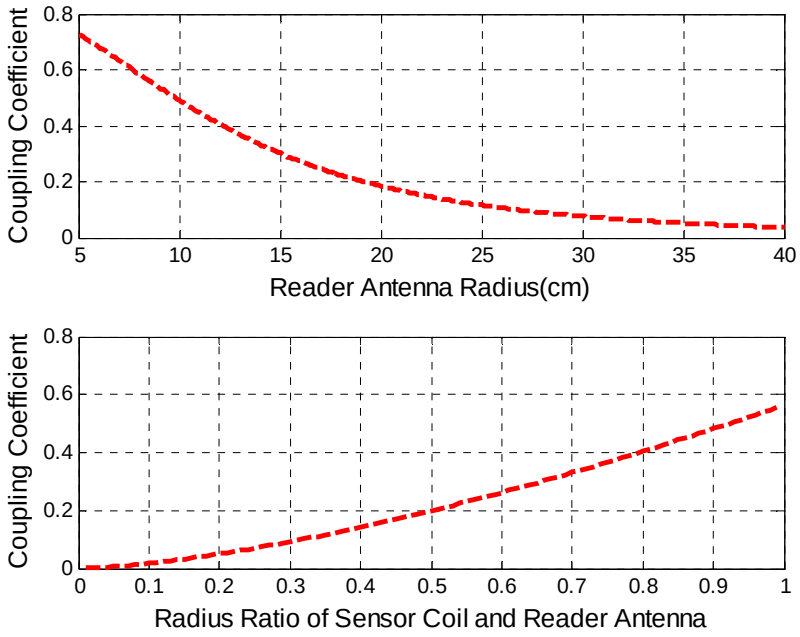

Figure 5.6 Coupling Coefficient *vs.* Reader Antenna Radius & Radius Ratio

5.3 Conclusions

In this section, the performance analysis of the passive wireless temperature sensor is investigated with respect to resonant frequency, *Q*-factor and coupling factor. Besides the parameters mentioned above, there is another solution --- capacitance compensation, which can be adopted to maximize reflected sensor impedance in order to make the resonant frequency detectable. That is, introduce a capacitance into the reader's side in order to make another resonant circuit, leaving the full sensor impedance changes occurring at the reader's side. However, this capacitor would need to change according to the resonant frequencies value for maximum efficiency, which may not be easily feasible. This in turn would require more sophisticated compensation architectures.

All in all, sensor simulation were preformed providing improvements, in order to achieve high performance wireless system, characterized with a high *Q*-factor and a maximized communication distance, which can be concluded as follows: to maximize sensor inductance, the radius ratio of the sensor inductor and reader coil, to minimize the sensor resistance, the radius of the reader antenna, reader inductance, or introduce reader capacitance compensation.

6 SENSOR FABRICATION

As a proof of concept experiment, sensor prototype fabrication is discussed in this Chapter. The Low Temperature Cofired Ceramic *(LTCC)* technology based on Green Tape is also proposed for sensor packaging. In addition, capacitance measurement and sensor calibration is given in the range from 20 °C to 235 °C.

6.1 Sensor Prototype

The sensor prototype and its equivalent circuit were shown in Figure 6.1. Here a spiral inductor with two turns was made of enamel-coated magnet copper wire, connected to the electrodes of the capacitor using *6041D* Ag paste. The diameter of the round copper wire, *2a,* is *0.674 mm*; the radius of the inductor, *R*, is *28.5 mm.* The area of the electrode plate, *A*, was $25mm^2$ and the thickness of dielectric material, *t,* was *0.480 mm*. In this figure, L_S indicates the sensor inductance, C_S means the sensor capacitor, R_S corresponds to the ohmic resistance in the sensor and Z_S demonstrates the impedance of this sensor prototype.

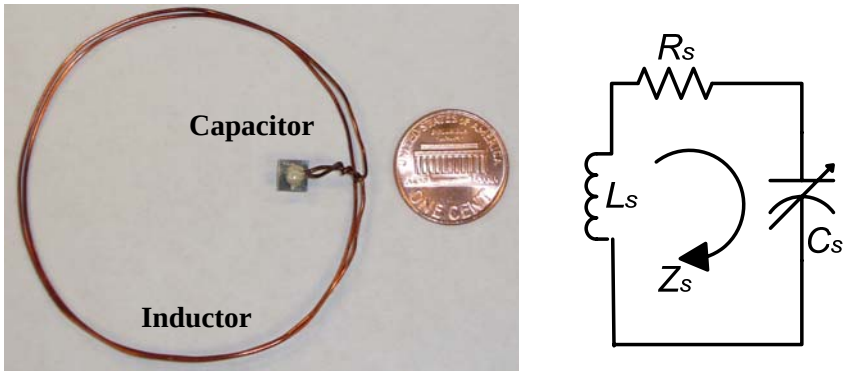

Figure 6.1 Sensor Prototype and Equivalent Circuit

6.2 Sensor Package

The Low Temperature Cofired Ceramic (*LTCC*) is a promising technology that produces multilayer circuits with the help of single tapes, which are used to apply conductive, dielectric and / or resistive pastes. These single sheets have to be laminated together and all fired in one step. This saves time, money and reduces circuit dimensions. Another great advantage of this technology is that every single layer can be inspected, and in the case of inaccuracy or damage, be replaced before firing. This prevents the need to manufacture a whole new circuit. Due to its low firing temperature (about 850°C), it is possible to use the low resistive materials like silver and gold instead of molybdenum and tungsten.

Due to its high density, high reliability, excellent performance and low cost interconnects package, Figure 6.2 shows the schematic sensor package using *LTCC*. The sensor package consists of two diaphragms, separated by temperature – dependent dielectric material, which is enclosed by two electrode plates that form a capacitor. The capacitor is electrically connected to a planar spiral inductor coil. These components form a passive *LC* resonator. The *LTCC* processing based on multiple sheets of Dupont 951 Green Tape™ is introduced in [68].

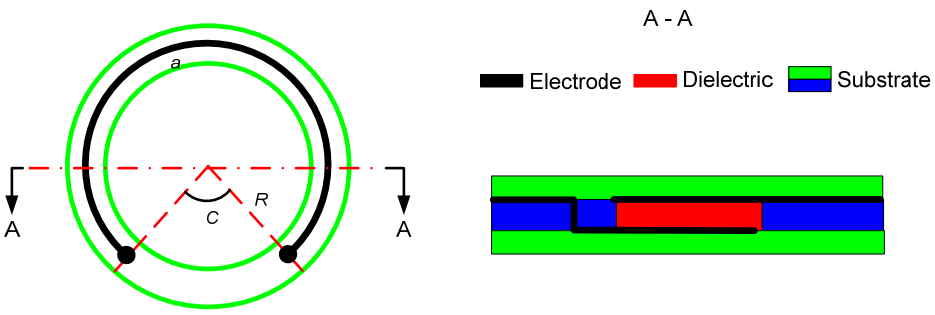

Figure 6.2 *LC* Sensor Package (Single Coil)

6.3 Capacitance Measurement

A circuit containing a resistance, an inductor and a capacitor is an electric analog to a simple harmonic oscillator, called *RLC* circuit. Discharging a capacitor through an inductor causes voltage and current oscillations. Capacitance can be measured using a *RLC* circuit by acquiring the resonant frequency. In this section, this measurement principle and experiment performing using a *RLC* circuit will be provided.

6.3.1 Oscillations of the RLC Circuit

In *RLC* circuit, the characteristic frequency f_0 of the oscillations depending on the capacitance C and inductance L can be expressed by equation 6-1:

$$f_0 = \frac{1}{2\pi\sqrt{LC}}. \qquad \textbf{6-1}$$

Since capacitors and inductors do not have ideal characteristics, the oscillations in the *LC* circuit are significantly damped. If the *RLC* circuit in the series is connected to a signal generator, the system cannot oscillate with characteristic frequency f_0, but it oscillates with frequency f that is "forced" by the generator. The impedance of the circuit is expressed as follows:

$$|Z| = \sqrt{R^2 + (X_L - X_C)} = \sqrt{R^2 + (2\pi fL - \frac{1}{2\pi fC})}. \qquad \textbf{6-2}$$

If $f>>f_0$, the impedance of the inductor and the amplitude of voltage on the inductor is much larger than the capacitor. However, if $f<<f_0$, impedance of the inductor and the amplitude of voltage on the capacitor is much larger than the inductor. At $f=f_0$, the impedance of the system is minimal, the amplitudes of the capacitor and inductor are equal and the circuit is in resonance.

Ohmic resistance of the circuit is an important influencing reason for the *RLC* damping, which can be shown in Figure 6.3. In this plot, parameters are used for a sensing area, *A,* of $25mm^2$, a thickness of the sensitive material, *t,* of *0.480mm,* a wire radius, *a,* of *0.337mm,* an inductor radius, *R,* of *8.5mm,* two turns of the inductor, the relative dielectric constant of *500,* and the ohmic resistance ranging from *50 ohm* to *1000 ohm.* As we see from this plot, when resistance reduces, the peak of voltage will not be easy to recognize.

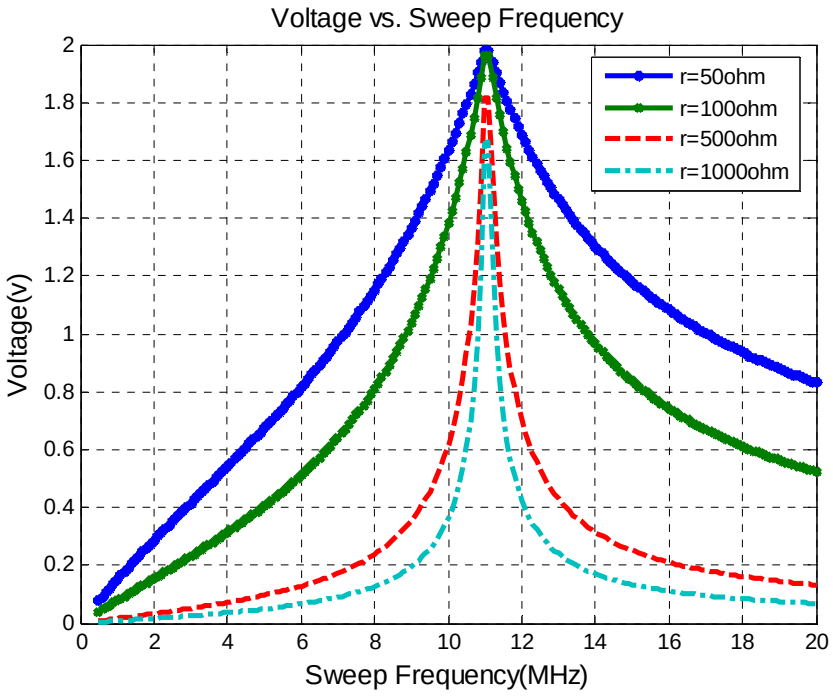

Figure 6.3 Voltage *vs.* Sweep Frequency

6.3.2 Performing the Experiment

An *Agilent 33220A 20MHZ* swept function generator, a *HEWLETT 54602B* packard oscilloscope and a *FLUKE 123* scope meter were used for this experiment. The impedance of the capacitor is

$$X_C = \frac{1}{2\pi jfC}. \qquad \textbf{6-3}$$

The impedance of the inductance is

$$X_L = 2\pi jfL. \qquad \textbf{6-4}$$

And the impedance of the parallel capacitor and inductance is

$$\frac{1}{Z_{LC}} = \frac{1}{X_C} + \frac{1}{X_L}. \qquad \textbf{6-5}$$

So the total impedance in the circuit is

$$Z = R + Z_{LC} = R + \frac{1}{2\pi jfC + \frac{1}{2\pi jfL}}. \qquad \textbf{6-6}$$

Sweeping the input signal in the *RLC* circuit produces a variation of the total impedance that will change according to environment temperature. Figure 6.4 shows the

simulation at a temperature interval of 20 °C and parameters are used the same as in Figure 6.3.

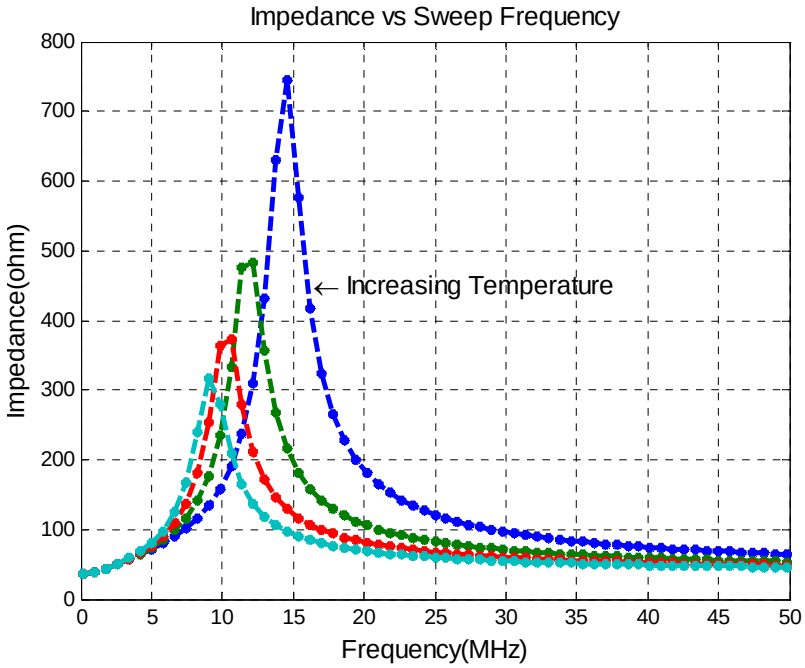

Figure 6.4 Impedance Variation

When the sweep frequency superposes the resonant frequency, the impedance will be maximal. At a certain temperature, the voltage variation of the capacitor as a function of the sweep frequency is illustrated in Figure 6.5.

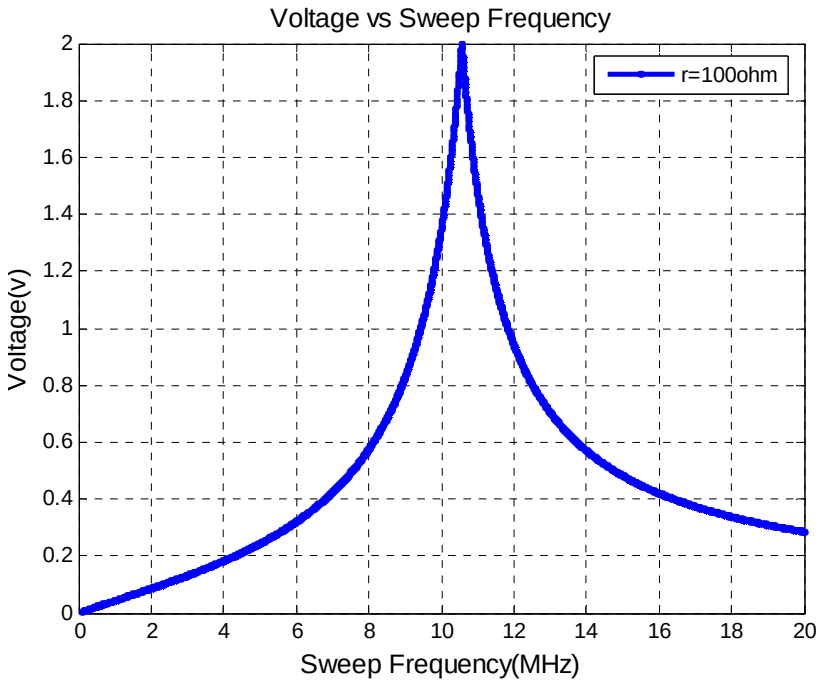

Figure 6.5 Voltage *vs.* Sweep Frequency

By using equation 6-1, the capacitance variation can be calculated for different temperatures, as illustrated in Figure 6.6. Here inductor of 0.68 μH and resistance of 100 Ω are used in this *RLC* measurement circuit.

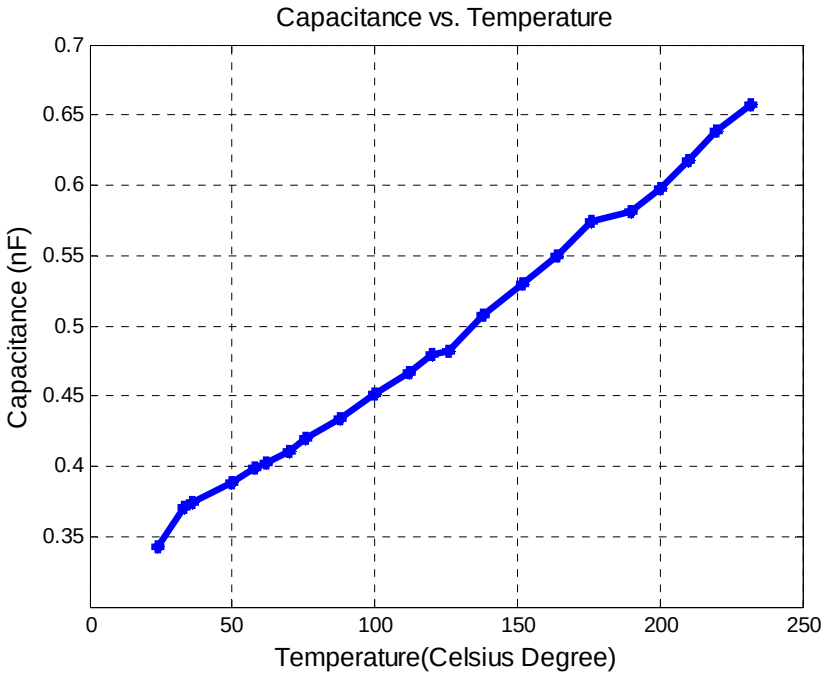

Figure 6.6 Capacitance *vs.* Temperature

6.4 Sensor Calibration

The *LC* temperature sensor was calibrated over a temperature range from 20ºC to 235ºC. A schematic principle of experiment set up is shown in Figure 6.7. Temperature sensor was immersed into an oil glass, which was put on the Hot Plate, providing the temperature range from room temperature to 450 ºC. The oil's temperature was measured by thermometers directly. At the same time, the antenna of the reader was laid outside of the glass jar, which transferred the temperature information to the reader. This information can be read out from the laptop in terms of resonant frequency.

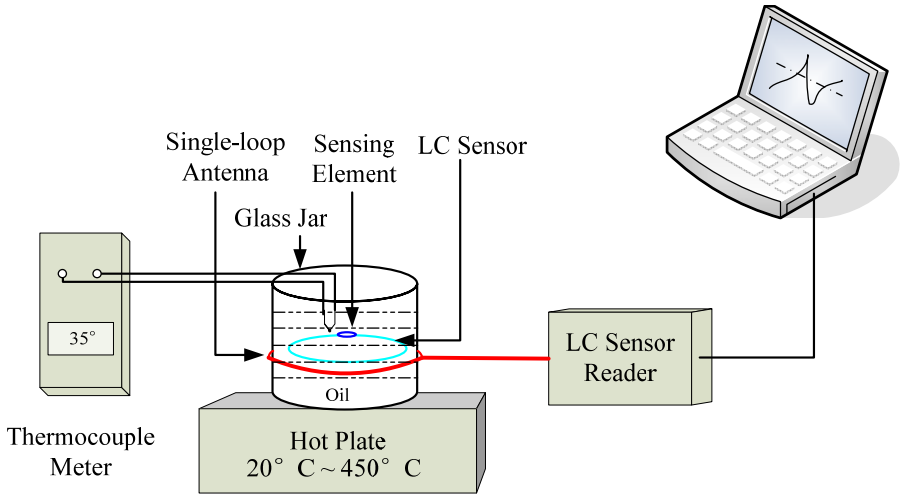

Figure 6.7 Principle of Sensor Calibration Experiment

Resonant frequency was recorded along with temperature variations, which is plotted in Figure 6.8. This proves that the *LC* temperature sensor made of a ferroelectric material is feasible for wireless temperature monitoring. The ferroelectric material of the capacitor is temperature dependent, that is, as the temperature increases or decreases, the dielectric constant will change correspondingly. This causes the capacitance variations along with temperature and then the resonant frequency is response to environmental temperature changes.

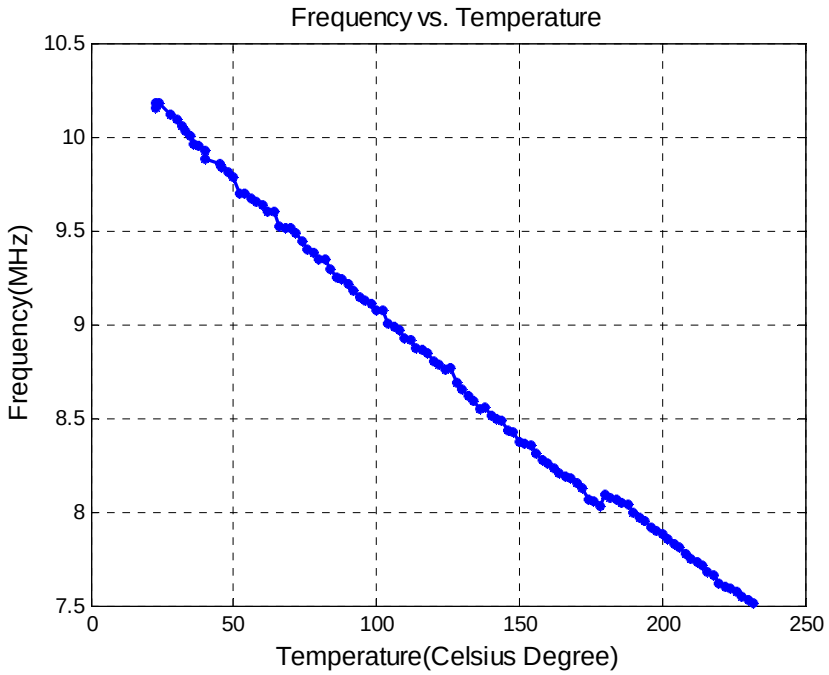

Figure 6.8 Sensor Calibration

6.5 Conclusions

In this Chapter, sensor prototype was fabricated to determine if a temperature sensitive element integrated with ceramic materials was feasible to monitoring high temperature in harsh environment. Sensor package based on the *LTCC* technology was proposed to produce a capacitor of high volumetric efficiency, good reliability, low cost and broad operation temperature range. In addition, experiments were performed for capacitance measurement and sensor calibration at temperatures ranging from 20 °C to 235 °C.

7 CONCLUSIONS AND FUTURE WORK

7.1 Conclusions

This research project has developed a novel passive wireless temperature sensor, being able to operate in harsh environments, for high temperature rotating component monitoring. A completely passive *LC* resonant telemetry scheme, which relies on a frequency shift output, has been integrated with the sensor, thereby eliminating the need for contacts, active elements, or power supplies within the sensor. Consisting of an inductor and a temperature-dependent capacitor, this high temperature sensor forms a *LC* circuit, whose resonant frequency shifts when the capacitance of the sensor changes in response to temperature.

Following a review of the state-of-the-art high temperature dielectric ceramics and substrates, the capacitor schematic design was presented based on temperature sensitive ferroelectric dielectrics. These dielectrics were found to exhibit linear changes in electrical properties when exposed to temperature varying environments. Based on capacitance and inductance modeling and simulation, sensor design and modeling was conducted subsequently in order to limit the resonant frequency to the appropriate scope.

Moreover, sensor performance was analyzed to optimize the sensor configuration, maximize sensing distance, *Q* factor and sensitivity. The sensor prototype was then successfully fabricated to prove the concept of a temperature sensing device using passive wireless communication. The Low Temperature Co-fire Ceramic (*LTCC*) technology based

on DuPont Green Tape ™ was proposed for sensor packaging. Finally, the sensor prototype was calibrated up to 235ºC.

Research contributions achieved by this project can be summarized as follows:

- An innovative passive wireless sensor scheme has been successfully demonstrated;
- High temperature sensitive materials and substrates were investigated and validated;
- Sensor performance were analyzed;
- The sensor prototype was developed and calibrated.

The temperature effect on *LC* planar resonator was fully investigated which disclosed a new potential application to monitor temperatures in harsh environments. The proposed temperature sensor is a simple planar structure which measures stable accurate temperature by a wireless and powerless feature, which enables a long-term temperature detection and integrated wireless communication.

The effective design of planar resonators for wireless sensing applications requires a process to obtain a geometry that optimizes application requirements. Modeling and simulation were performed in order to minimize sensor size, maximize the detection distance, quality factor, and sensor sensitivity.

7.2 Future Work

Some research could be expanded in the future:

- Extend the communication distance of the temperature sensor;
- Analyze the temperature-dependent inductance and resistance in order to calibrate the sensor much more accurately;
- Realize sensor packaging based on proposed *LTCC* technology.

REFERENCES

[1] Yibing Zhang, Gary Pickrell, Bing Qi, Russell G.May, and Anbo Wang, "Single-crystal sapphire-based optical high-temperature sensor for harsh environments", *Optical Engineering*, vol. 43, 2004, pp.157-164.

[2] Darrin J. Young, Jiangang Du, Christian A. Zorman, Wen H. Ko, "High-Temperature Single-Crystal 3C-SiC Capacitive Pressure Sensor", *IEEE sensors journal*, vol. 4, August 2004, pp.464-470.

[3] David A. Stubbs and Rollie E. Dutton, "An Ultrasonic Sensor for High-Temperature Materials Processing", *Journal JOM*, vol. 48, 1996, pp. 29-31.

[4] Otto J. Gregory and Tao You, "Ceramic Temperature Sensors for Harsh Environments", *IEEE Sensor Journal,* vol. 5, October 2005, pp. 833-838.

[5] J. Goetz, "Sensors that can take the heat", *Sensors*, June 2000, pp. 20–38.

[6] Lemi Toygur, "Interface Circuits in SOI-CMOS for High-temperature Wireless Micro Sensors," Ph.D. Dissertation, Case Western Reserve University, OH, January 2004.

[7] P. G. Neudeck, R. S. Okojie, and L.-Y. Chen, "High temperature electronics— A role for wide bandgap semiconductors?", *Proceedings of IEEE*, vol. 90, June, 2002, pp. 1065–1076.

[8] G.W. Hunter, P.G. Neudeck, L-Y. Chen, et al. "SiC-Based Schottky Diode Gas Sensors", *Materials Science Forum,* vols. 264-268, 1998, pp. 1093-1096.

[9] J. B. Bates, G. R. Gruzalski, and C. F. Luck, “Rechargeable solid state lithium microbatteries”, in *Proc. IEEE Micro Electro Mechanical Systems, MEMS* ’93, Fort Lauderdale, FL, February 1993, pp. 82–86.

[10] D. Linden, Handbook of Batteries, 2nd ed. New York: McGraw-Hill, 1994.

[11] T. Toriyama, M.Yajima, and S. Sugiyama, “Thermoelectric micro power generator utilizing self standing polysilicon-metal thermopile”, *in Proc. 14th IEEE International Conference on Micro Electro Mechanical Systems*, 2001, pp. 562–565.

[12] S. Chatzandroulis, D. Tsoukalas, and P. A. Neukomm, “A miniature pressure system with a capacitive sensor and a passive telemetry link for use in implantable applications”, *J. Microelectromech. Syst.*, vol. 9, March 2000, pp. 18–23.

[13] C. Hierold, B. Clasbrumme, D. Behrend, T. Scheiter, M. Steger, K. Oppermann, H. Kapels, E. Landgraf, D. Wenzel, and D. Etuodt, “Implantable low power integrated pressure sensor system for minimal invasive telemetric patient monitoring”, *in Proc. IEEE Micro Electro Mechanical Systems, MEMS* ’98, 1998, pp. 568–573.

[14] K. Stangel, S. Kolnsberg, D. Hammerschmidt, B. J. Hosticka, H. K. Trieu, and W. Mokwa, “A programmable intraocular CMOS pressure sensor system implant”, *IEEE J. Solid-State Circuits*, vol. 36, July 2001, pp.1094–1100.

[15] E. Magison, “Temperature measurement-physical principles underlie the four common methods”, *Industrial temperature measurement*, November 2001, pp. 39-41.

[16] R. E. Bentley, “Temperature and humidity measurement”, Handbook of temperature measurement, vol. 1, Singapore; New York, Springer, 1998.

[17] M. R. Werner, and W. R. Fahrner, “Review on materials, microsensors, systems, and devices for high-temperature and harsh-environment applications”, *IEEE trans*. Ind. Electron., vol. 48, no. 2, April 2001, pp. 249-257.

[18] J. R. Leigh, Temperature measurement and control, Chapter 5, Perter Peregrinus Ltd, London, United Kingdom, 1988.

[19] G. B. Lu, and H. C. Yan, “Concurrent measurements of temperature and soot concentration of pulverized coal flames”, *Instrumentation and Measurement Technology Conference*, 2001. IMTC 2001, Proc. the 18th IEEE, vol. 2, pp. 1221 – 1226.

[20] J. Castrellon, G. Paez, and M. Strojnik, “Radiometric analysis of a fiber optic temperature sensor”, *Opt. Eng*. vol. 41, no. 6, June, 2002, pp. 1255-1261.

[21] K. M. Koo, J. H. Kim, S. B. Kim, H. D. Kim, and D. Y. Ko, “Ultrasonis thermometry system for measuring very high temperatures using high resolution signal processing”, *Proc. IECIC 2001*, August 2001.pp. 229-232.

[22] D. P. Dewitt and G. D. Nutter, Theory and practice of radiation thermometry, John Wiley&Sons, Inc. New York, 1988.

[23] B. E. Adams, “Optical fiber thermometry for use at high temperatures”, In J. F. Schooley, editor, Temperature: its measurement and control in science and industry, vol. 6 Amer. Inst. Phys. New York, 1992, pp. 739-743.

[24] R. O. Claus, M. F. Gunther, A. Wang, K. A. Murphy, “Exitrinsic Fabry-Perot sensor for strain and crack opening displacement measurement from –200 to 900°C”, *J. of Smart Materials and Structures*, vol.1, no.3, 1992.

[25] H. Xiao, J. Deng, R. May, and A. Wang, "Single crystal sapphire fiber-based sensors for high-temperature applications", *Proc. SPIE 3201,* Bonston, MA, September 19, 1999.

[26] M. Sun, "Fiberoptic thermometry based on photoluminescent decay times", In J. F. Schooley, editor. *Temperature: its measurement and control in science and industry,* vol. 6, Amer. Inst. Phys, New York, 1992, pp. 715-719.

[27] Aizawa, H., Katsumata, T., Komuro, S., Morikawa, T., Ishizawa, H., Toba, E., "Fiber-optic thermometer for high temperature measurement", *SICE-ICASE, International Joint Conference,* 2006.

[28] B. W. Noel, W.D. Turley, W. Lewis, K. W. Tobin, and D. L. Beshears, "Phosphor thermometry on turbine-engine blades and vanes", In J. F. Schooley, editor. *Temperature: its measurement and control in science and industry*, vol. 6, Amer. Inst. Phys, New York, 1992, pp.1249-1254.

[29] A. B. Murphy, "Laser-scattering temperature measurements of a free burning arc in nitrogen", *J. Phys. D: Appl. Phys*, 27, 1994, pp. 1492-1498.

[30] O. Iida, T. Iwamura, K. hashiba, and Y. Kurosawa, "A fiber optic distributed temperature sensor for high-temperature measurements", In J. F. Schooley, editor. *Temperature: its measurement and control in science and industry,* vol. 6, Amer. Inst. Phys, New York, 1992, pp. 745-749.

[31] Alfred Pohl, "A Review of Wireless SAW Sensors", *IEEE Transactions on Ultrasonics, Ferroelectrics, and Frequency Contorl*, vol. 47, no.2, March 2000, pp.317-332.

[32] Shou-Qi Wang, Jiro Harada and Satoshi Uda, "A Wireless Surface Acoustic Wave Temperature Sensor Using Langasite as Substrate Material for High-Temperature Applications", *The Japan Society of Apply Physics*, vol. 42, 2003, pp. 6124–6127.

[33] Gernot Schimetta, Franz Dollinger, and Robert Weigel, "A Wireless Pressure-Measurement System Using a SAW Hybrid Sensor", *IEEE Transactions on Microwave Theory and Techniques*, vol.48, no.12, December 2000, pp. 2730-2735.

[34] M. S. Nieuwenhuizen, A. J. Nederlof and A. Coomans, "A SAW gas sensor for NO_2. Chemically immobilized phthalocyanines as chemical interface, *Fresenius", Journal of Analytical Chemistry,* vol. 330, January 1998, pp. 123-124.

[35] F. Seifert and R. Weigel, "SAW-based radio sensor and communication techniques", *Proceedings of the 27th European Microwave Conference, Jerusalem, Israel*, 1997, pp. 1323–1346.

[36] C. Calend, E. Verona and V. I. Anisimkin, "Surface Acoustic Wave Humidity Sensors: a Comparison between Different Types of Sensitive Membrane", *Smart Material Structure*, vol. 6, 1997, pp.707-715.

[37] Olivier Chevalerias, Terence O'Donnell, Daithí Power, Neil O'Donavan, Gerald Duffy, Gary Grant, and Seán Cian O'Mathuna, "Inductive Telemetry of Multiple Sensor Modules", *IEEE Pervasive Computing*, vol.4, no.1, March 2005, pp.46-52.

[38] J.M. English, M.G. Allen, "Wireless Micromachined Ceramic Pressure Sensors", Proceedings IEEE MEMS '99, 1999, pp. 511-516.

[39] Michael A. Fonseca, Jennifer M. English, Martin von Arx and Mark G. Allen, "Wireless Micromachined Ceramic Pressure Sensor for High-Temperature Applications", *Journal of Microelectromechanical systems*, vol.11,no.4, August 2002, pp.337-343.

[40] E.D. Birdsell, J. Park, M.G. Allen, "Wireless Ceramic Sensors Operating in High Temperature Environments", *40th AIAA/ASME/SAE/ASEE Joint Propulsion Conference*, Fort Lauderdale, FL, July 2004.

[41] E.D. Birdsell, M.G. Allen, "Wireless Chemical Sensors for High Temperature Environments", *Solid-State Sensors, Actuators, and Microsystems Workshop,* 212 Hilton Head Island, South Carolina, June 4-8, 2006.

[42] Timothy J. Harpster, Sébastien Hauvespre, Mehmet R. Dokmeci and Khalil Najafi, "A Passive Humidity Monitoring System for In Situ Remote Wireless Testing of Micropackages", *Journal of Microelectromechanical System*, vol. 11, No. 1, February 2002, pp. 61-67.

[43] Frederick W. Grover, "Inductance Calculations: Working Formulas and Tables", Dover Publications, Inc., New York, 1946.

[44] Sunderarajan S. Mohan, Maria del Mar Hershenson, Stephen P.Boyd, and Thomas H.Lee, "Simple Accurate Expressions for Planar Spiral Inductances", *IEEE, Journal of Solid-State circuits*, vol.34, pp.1419-1424.

[45] Klaus Finkenzeller, RFID Handbook, 2nd Ed., John Wiley & Sons, 2003.

[46] DuPont Thick Film Material System---AlN, Manual.

[47] http://www.precision-ceramics.co.uk.

[48] Heng Ban, "Nover Corrosion Sensor for Advanced Energy Systems", Report, University of Alabama, Birmingham, Department of Mechanical Engineering.

[49] http://www.goodfellow.com.

[50] Heng Ban, Zuoping Li, "A Novel Sensor and Measurement System for Fireside Corrosion Monitoring in Coal-Fired Boilers", Final Technical Report, March 2003.

[51] http://www.precision-ceramics.co.uk

[52] J. M. Herbert, Ferroelectric Transducers and Sensors, Gordon and Breach, London, 1982.

[53] R. C. Buchanan, ed., Ceramic Materials for Electronics - *Processing, Properties and Applications* (Marcel Dekker, New York, 1986).

[54] L. M. Levinson, ed., Electronic Ceramics Properties, Devices and Applications (Marcel Dekker, New York, 1987).

[55] J. Moulson and J. M. Herbert, Electroceramics, Materials, Properties, and Applications (Chapman and Hall, London, 1990).

[56] Leppavuori S.; Lozinski A.H.;Uusimaki A, "A Thick-film Pyroelectric PLZT Ceramic Sensor", Sensors and Actuators, A: Physical, vol. 47, no. 1, March 1995 , pp. 391-394(4).

[57] Ahmad Safari, Rajesh K. Panda, and Victor F. Janas, "Ferroelectric Ceramics: Processing, Properties & Applications", Rutgers University, Piscataway NJ 08855, USA.

[58] R.A.Dorey, and R.W.Whatmore, "Pyroelectric PZT/PMNZTU Composite Thick Films", Journal of the European Ceramic Society, vol. 25, Issue 12, 2005, pp. 2379-2382.

[59] Y. Xu, Ferroelectric Materials and their Applications (North Holland, Amsterdam, 1991)

[60] R.E. Eitel, C.A. Randall, T.R. Shrout, P.W. Rehrig, W. Hackenberger, and S.-E. Park, "New High Temperature Morphotropic Phase Boundary Piezoelectrics Based on Bi (Me)O3-PbTiO3 Ceramics,". *Appl. Phys*. Pt.1 40, 2001, pp. 5999-6002.

[61] Blanco, J.L.Heiras and J.M.Siqueiros, "Electrical Properties of PZT Thin Films", *IEEE Proceedings*, 2001.

[62] I.A. Santos, C. Endo, A.L. Zanin, M.H. Lente, J.A. Eiras, D. Garcia, "Hot-Pressed Transparent PLZT Ceramics from Low Cost Chemical Processing", *Materials Research,* vol. 4 no.4, São Carlos, October 2001.

[63] Bruno Acácio Menegazzo, José Antonio Eiras, "Preparation of Coprecipitated Ferroelectric Ceramic Powders by Two-Stage Calcination", *Journal of the American Ceramic Society,* vol. 76 (11), 1993, pp. 2734–2736.

[64] Tadashi Takenaka, Hiroki Korniya and Koichiro Sakata, "PbZrO3-Based Composite Pyroelectric Ceramics", *IEEE proceedings*, pp. 370-373.

[65] Radheshyam Rai, Seema Sharmab, R.N.P. Choudhary, "Structural and dielectric properties of Bi modified PLZT ceramics," *Solid State Communications*, vol.133, 2005, pp. 635–639.

[66] Surya Musunuri, Patrick L. Chapman, Jun Zou, and Chang Liu, "Design Issues for Monolithic DCDC Converters", *IEEE Transactions on Power Electronics*, vol.20, no.3, May 2005, pp.639-649.

[67] K. Finkenzeller, RFID Handbook, Fundamentals and Applications in Contactless Smart Cards and Identification, 2nd ed., John Wiley & Sons Ltd, 2003.

[68] Green Tape Material System， Design and Layout Guidelines, Dupont Applied Technologies Group, pp.1-17.